



Politecnico di Torino

Corso di Laurea Magistrale in Ingegneria Biomedica

**Experimental biaxial mechanical characterization of soft
biological tissues for cardiac bioprostheses design**

Author:

Andrea Tancredi Lugas

Supervisors:

Prof. Alberto Audenino

Dr. Mara Terzini

Index

Abstract	1
1. Introduction.....	3
1.1. The pericardium	3
1.1.1. Anatomy and histology	3
1.1.2. The pericardium as a biomaterial.....	5
1.2. Heart Valves	5
1.2.1. Anatomy and histology	5
1.2.2. Functioning during the heart cycle.....	6
1.2.3. Diseases.....	8
1.3. Prosthetic heart valves.....	9
1.3.1. Mechanical heart valves.....	9
1.3.2. Biological heart valves.....	9
1.4. The aorta.....	10
1.4.1. Anatomy and histology	10
1.4.2. Diseases.....	12
1.4.3. Aorta as a biomaterial	13
1.5. Treatments	14
1.5.1. Glutaraldehyde	15
1.5.2. Acid-free glyoxal	15
1.6. Mechanical characterization.....	16
1.6.1. Control loop tuning	18
2. Materials and methods	20
2.1. Specimens preparation	20
2.2. Thickness measurement	20
2.2.1. CNC controlled scanning probe	20
2.2.2. Sample holder	22

2.2.3. Measure procedure.....	23
2.2.4. Thickness values	24
2.3. Biaxial mechanical testing.....	24
2.3.1. System description	24
2.3.2. Specimen mounting.....	26
2.3.3. WinTest.....	28
2.3.4. Load-controlled biaxial protocol.....	29
2.3.5. Displacement-controlled protocol.....	32
2.3.6. Markers segmentation	34
2.3.7. Mechanical indexes and statistical analysis	38
3. Results and discussion	41
3.1. Stress-strain curves.....	41
3.1.1. Literature comparison	43
3.2. Stiffness estimation and statistical analysis.....	45
3.2.1. The Aorta	45
3.2.2. The pericardium	48
4. Conclusions.....	52
Bibliography.....	54

Abstract

Glutaraldehyde (GLU) treatment for biological tissues represents the current standard for cardiac bioprostheses design. An acid-free glyoxal (GAF) fixative devised by the Department of Medical Sciences (University of Turin) allows the obtaining of a more durable tissue, being less prone to calcification after implantation in the human body environment. However, an essential requirement in cardiac bioprostheses design is the mechanical performance of the starting material, and each fixation treatment may compromise the tissue structure, consequently deteriorating its mechanical properties. Therefore, the aim of this thesis is to develop a mechanical biaxial testing protocol and characterize the mechanical properties of GAF-treated and GLU-treated tissues comparing their performances.

Specimens of bovine pericardium and porcine aorta treated with both methods were prepared and stored in physiological saline solution at 4°C. Before testing, the samples thickness was measured detecting a 25-points matrix in the central region of each specimen using a CNC controlled scanning probe. Specimens were then cut in 15x15 mm² squares with the apex-base and circumferential (pericardium) or longitudinal and circumferential (aorta) directions parallel to the edges. 16 equally spaced sutures were placed on the edges of the specimen and connected to 4 grip fixtures on the planar test bench (TA Instruments). Finally, small markers were drawn in the central region of the specimens, which were filmed during the stress protocol for strain computations. The specimens were immersed in saline solution at 37 °C throughout the test.

Load-controlled and displacement-controlled protocols were devised to explore the entire range of physiologic loadings and to obtain adequate data for literature comparisons and for future constitutive modeling. Stress-strain curves were used to determine the tissues elastic modulus along the two loading directions, i.e. the curve slope. This mechanical index is crucial to establish whether GAF-treated and GLU-treated pericardium and aorta have comparable mechanical properties and which treatment produces a tissue with a mechanical response more similar to the native one when subjected to physiological-like stresses. The data acquired from the test bench and from the video recording of the tests were elaborated using MATLAB custom routines. The such obtained stress-strain curves were compared with other curves from previous works on fresh pericardium and aorta and the trends resulted to be very similar, showing that the treatments do not produce massive changes in the mechanical properties of the tissues.

A three-way ANOVA was performed using treatments, directions and different cycles of the protocol as independent variables and the slope as dependent variable. The dependence of the stiffness on the directions was not determined. This can be explained with the fact that the test axes were not aligned

with the collagen fibers directions, but with the anatomical directions of the tissues, which do not provide significative information about mechanical properties of the specimens. However, this work provided a reliable biaxial displacement-controlled mechanical testing protocol for soft tissue which can be combined with other techniques for future investigations. Moreover, it has been proven that the treatment affects the stiffness of the tissues. In details, pericardium is stiffer when treated with acid-free glyoxal, while aorta have a greater elastic modulus when treated with glutaraldehyde.

1. Introduction

1.1. The pericardium

1.1.1. Anatomy and histology

The heart is surrounded by a membrane called pericardium or pericardial sac. Its shape and dimensions are the same as the heart, that moves inside it during the heartbeat. Various studies have attributed to the pericardium several functions, including protection of the heart from infections, over-dilatation or adhesion to surrounding tissues and maintenance of the heart in its position.¹

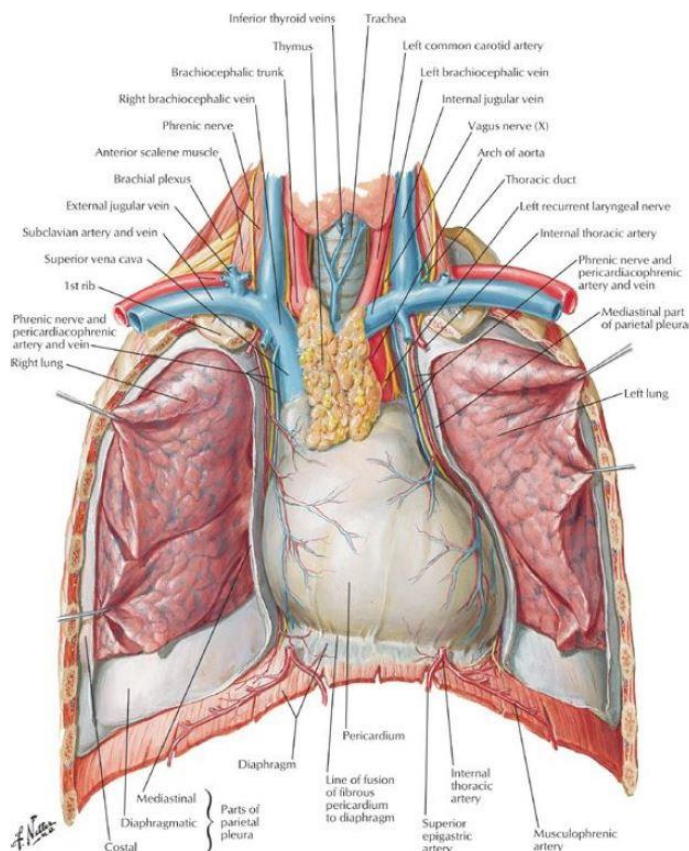


Figure 1.1 - Heart *in situ*²

The pericardium is distinguished in serous pericardium (serosa) and fibrous pericardium (fibrosa).

The serosa surrounds the heart and is divided in two sheets: the visceral pericardium and the parietal pericardium. The visceral pericardium is composed of a single layer of mesothelial cells and a thin layer of connective tissue, it is also referred to as epicardium and it is part of the heart wall.³ The parietal pericardium is made of flat or cubic mesothelial cells and a layer of connective tissue rich in structural proteins (collagen and elastin), fused with the fibrosa. The two layers can slide over

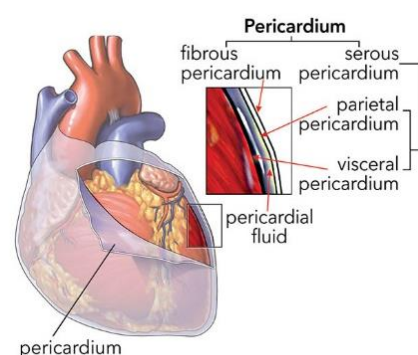


Figure 1.2 - Pericardium layers

each other because of a small amount of pericardial fluid contained in a cavity that separates them, referred to as *cavum pericardii*.

The fibrosa is more resistant and less extensible than the serosa. Its inner surface is fused with the parietal pericardium and cannot be separated from it, its external surface is covered by the epicardial connective tissue layer.⁴ The fibrous pericardium has a cellular component, composed of fibroblasts, and an extracellular matrix (ECM). The fibroblasts are the main cells of connective tissues and can synthesize all the components of the ECM, which are mostly collagen types I and III in the pericardium.⁵

ECM in turn can be distinguished in two components: the ground substance and the structural proteins. The ground substance influences tissue development, movements and proliferation. It is a gel-like homogenous transparent amorphous substance made of two classes of macromolecules: the proteoglycans and the glycoproteins. The structural proteins (collagen and elastin) are responsible for the tissue mechanical properties.

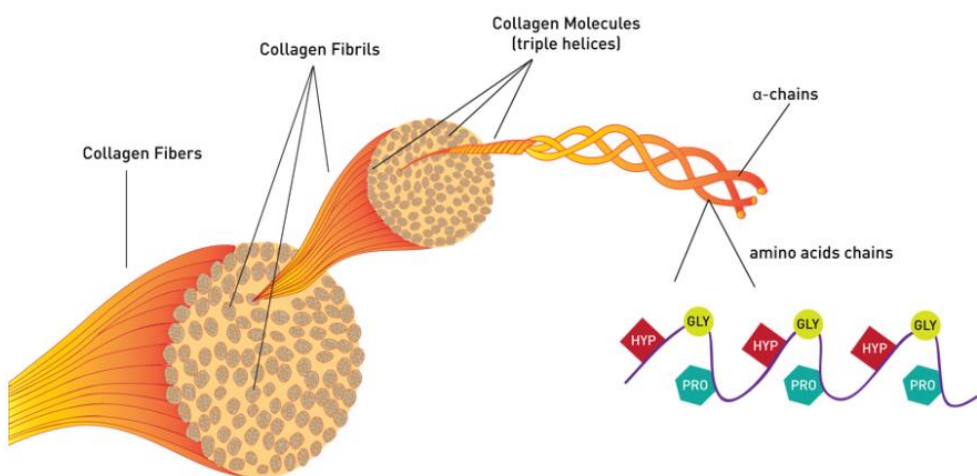


Figure 1.3 - Structure of the collagen fibers⁶

The collagen is organized in chains wrapped together forming a triple-helix structure referred to as tropocollagen. These units associate with each other to form fibrils, which form collagen fibers. Twenty-eight types of collagen have been described so far⁷; in bovine pericardium the collagen component is for 90% type I and for 10% type III.⁸

The tropoelastin is a precursor of elastin synthesized by fibroblasts. It forms polymeric fibers linked with covalent bonds (cross-link). The elastin allows the tissue to recover its shape after a deformation.

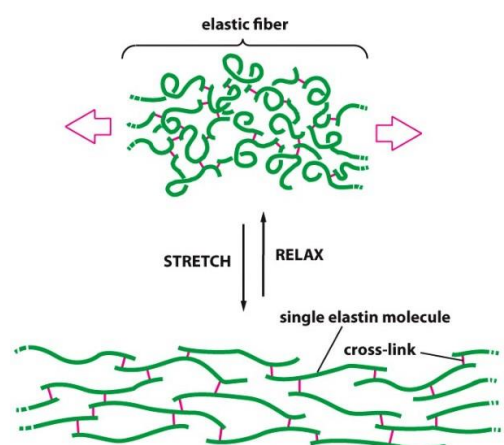


Figure 1.4 Structure of the elastin molecule

1.1.2. The pericardium as a biomaterial

Pericardium has been used so far for reconstructive surgery of the ligaments in hands and knees, tissue engineering, various types of prostheses such as patches for vaginal and abdominal wall reparation or tracheoplasty, several cardiac diseases treatments like postinfarction septal defects, reconstruction of mitral valve annulus, outflow obstruction. However, the main applications of pericardium as a biomaterial remain the design of prosthetic vascular grafts and, more often, heart valves.^{9,10}

Bovine pericardium proved to be a valid material for this purpose and some studies demonstrated that it allows a better hemodynamics than porcine aortic valve as a bioprosthesis. Moreover, the superior amount of collagen would positively influence the duration of the valve after implantation.¹⁰ Before implantation, the pericardium must be decellularized to remove antigenic elements, while preventing mechanical properties of the tissue. Currently used decellularization techniques and possible alternatives will be detailed below.

1.2. Heart Valves

1.2.1. Anatomy and histology

The heart has four valves:

- the mitral valve between the left atrium and ventricle;
- the tricuspid valve between the right atrium and ventricle;
- the pulmonic valve and the aortic valve respectively between the right and left ventricle and the major blood vessels leaving the heart.

The mitral and the tricuspid valves are called atrioventricular due to their location in the heart, while the pulmonic and aortic valve are called semilunar because of their shape.

Each valve is made of thin leaflets (or cusps) which allow the valves to open and close to let the blood flow in the desired direction and avoid backward flows during the different phases of cardiac cycle. The tricuspid, pulmonic and aortic valves have three cusps, the mitral (also referred to as bicuspid valve) has two. Atrioventricular valves are supported by fibrous strings referred to as chordae tendineae and by papillary muscles. Semilunar valves do not need this type of structure because the leaflets are more stable and support each other.¹¹

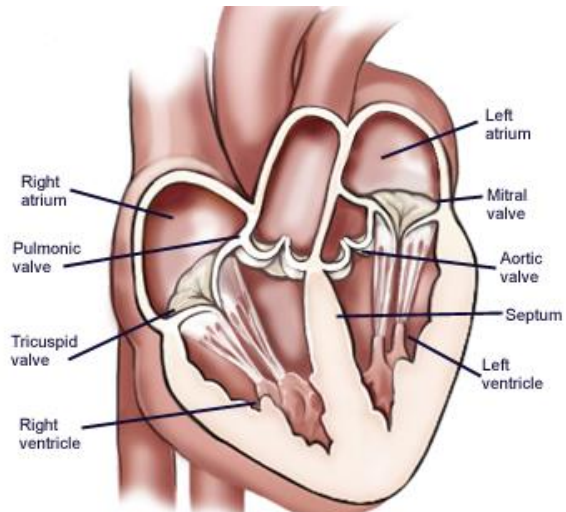


Figure 1.5 - Heart valves

All the valves are mainly made of a collagenous layer referred to as fibrosa and of a looser structure called serosa. The cusps are attached to a structure, the annulus, which is composed of connective tissue. The fibrosa is covered by connective tissue (a continuation of the arterial intima or ventricular endocardium) which contains elastic sheets. The elastic layers are thicker on the outflow surface and thin near the tip of the valve.¹²

1.2.2. Functioning during the heart cycle

Relaxation and contraction of heart chambers are called diastole and systole respectively and both atria and ventricles undergo these phases.

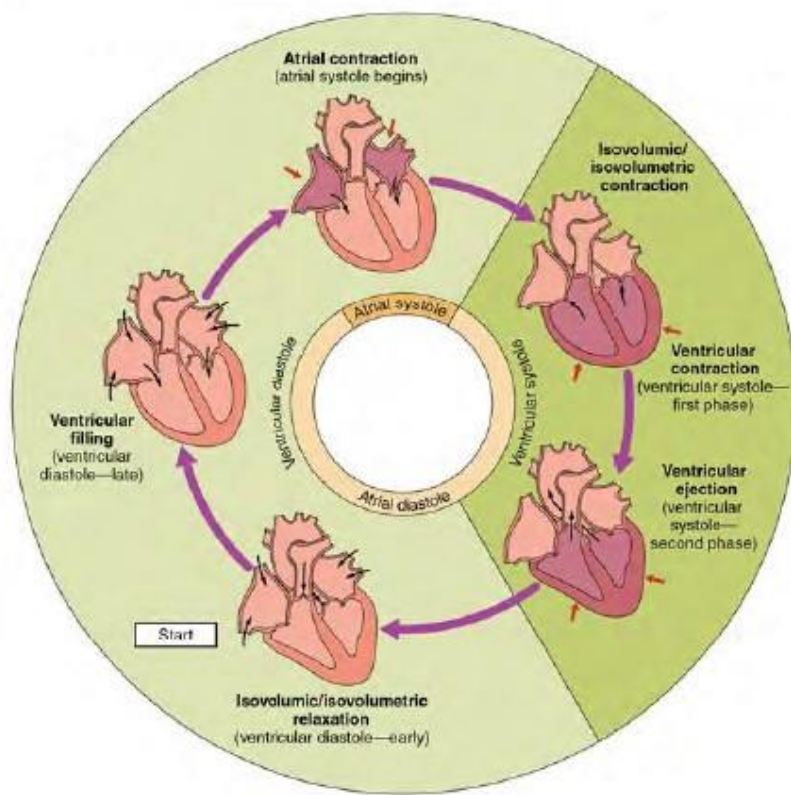


Figure 1.6 - Cardiac cycle³

Atrial diastole

At the beginning of the cardiac cycle all the chambers are relaxed, and the blood is flowing in the left atrium from the pulmonary veins and in the right atrium from the venae cavae and the coronary sinus. The ventricles are filled until 70-80% of their capacity through the atrioventricular valves which are both open. The semilunar valves are closed during this phase to avoid backward flow in the ventricles from the pulmonary trunk and the aorta.

Atrial systole

The remaining 20-30% of the ventricle is filled during the atrial systole. Atria contract and the blood flows through the mitral and tricuspid valves from the atria to the ventricles.

Ventricular systole

The ventricular contraction can be divided in isovolumic contraction and ventricular ejection. During the first phase the ventricles contract and the pressure in the chambers rises above that in the atria, closing the atrioventricular valves. Semilunar valves are still closed; therefore, blood is not flowing out of ventricles and the volume remains constant. When the pressure overcomes that of the pulmonary trunk and the aorta, the aortic and pulmonary valves open and the blood is ejected out of the ventricles.

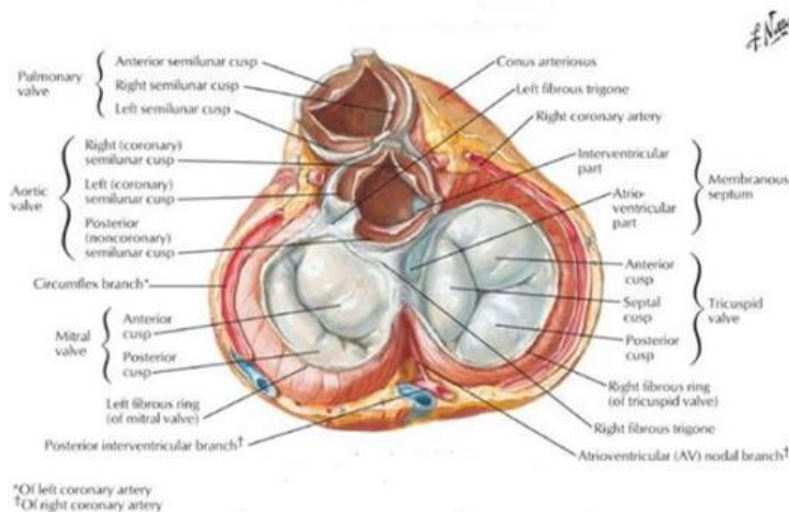


Figure 1.7 - Heart valves during ventricular ejection²

Ventricular diastole

During the early phase of ventricular diastole, the semilunar valves close to prevent backflow and the atrioventricular valves remain closed. This phase is called the isovolumic ventricular relaxation. When the pressure in the ventricles drops below that in the atria, the mitral and tricuspid valves open and let the flow fill the ventricles again.

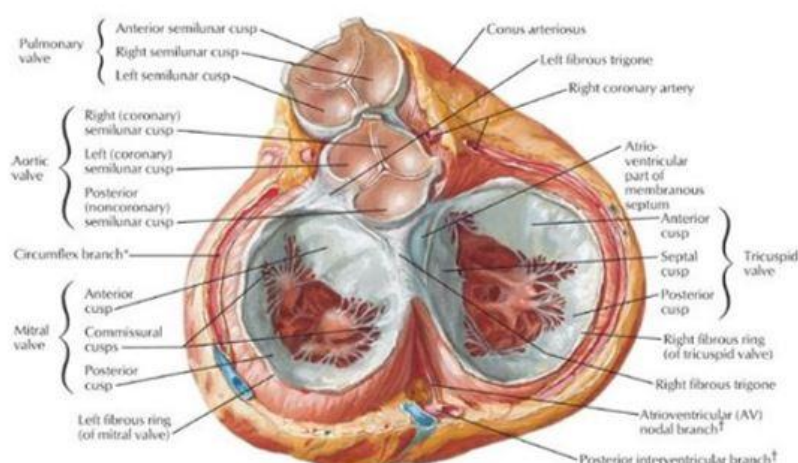


Figure 1.8 - Heart valves during ventricular diastole²

1.2.3. Diseases

The disease of the heart valves can be distinguished in two types: stenosis and insufficiency. The stenosis is an incomplete opening of the valve and limits the blood flow, the insufficiency is an incomplete closing of the valve and allows backflow. These diseases could occur separated or at the same time and can be congenital or caused by degeneration, ischemia or traumas.

Most frequently, diseases occur in the left atrium and ventricle, where the pressure is normally higher and more critical. The main valvular diseases are therefore aortic and mitral stenosis and insufficiency.

Mitral stenosis

Mitral stenosis consists in a narrowing of the mitral orifice that brings to a decrease of cardiac flow rate during diastole. Usually it is due to rheumatic disease, which causes deformation and shortening of the leaflets.

Mitral insufficiency

If the mitral valve is insufficient the blood can flow back from the left ventricle to the left atrium during diastole. This results in an increase in ventricular volume to supply the correct flow rate, and the ventricle undergoes dilatation and hypertrophy.

Aortic stenosis

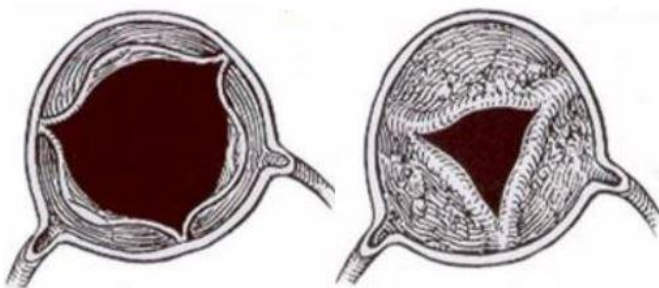


Figure 1.9 - Open aortic valve: normal (left) and stenotic (right)

The narrowing of aortic valve causes an increase in the resistance of the valve itself to blood flow from the left ventricle to the aorta, during systole. Subsequently, left ventricle undergoes hypertrophy. It can be caused by rheumatic fevers and congenital anomalies.¹³

Aortic insufficiency

A certain amount of blood flows back from aorta to left ventricle during diastole. This disease could be caused by deformation or shortening of the cusps, bacterial endocarditis or congenital disorders.

Aortic valve diseases are usually treated by replacing the native valve with a prosthetic one.¹⁴

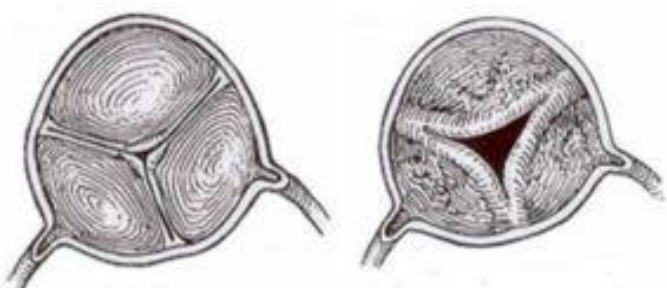


Figure 1.10 - Closed aortic valve: normal (left) and insufficient (right)

1.3. Prosthetic heart valves

1.3.1. Mechanical heart valves

Mechanical valves are implanted surgically and can be made of different materials such as stainless steel, ceramic or pyrolytic carbon.¹⁴ Prostheses of different shapes are currently commercially available:

- Ball valves are made of a silicone ball, a polymeric ring and a metallic cage. The ball occludes the valve when it is adjacent to the ring.
- Disc valves are comprised of a pyrolytic carbon-coated graphite disc which rotates between two pins in the metallic housing.
- Bileaflet valves have two semilunar leaflets, when the valve is open the blood flows through one central wide region and two lateral narrow regions.

Mechanical prostheses are thrombogenic, thus it is required a life-long anticoagulant treatment for the patient after the implantation. However, they can last much longer than biological prostheses (up to 25-30 years).¹⁴⁻¹⁶



Figure 1.11 - Ball valve (A), disc valve (B), bileaflet valve (C)¹⁷

1.3.2. Biological heart valves

The potential risks of long-term anticoagulant treatment led to the use of biological prostheses. Indeed, biological prostheses are not thrombogenic and do not require life-long treatments. Their shape is very similar to the native valves which should be replaced. The issues which could occur after implantation are related to rejection; to avoid it, tissues must be decellularized as pointed out above.

Biological valves can be divided according to their provenience in the following categories.¹⁶

- Homograft valves, from human cadavers.
- Autograft valves: the aortic valve is replaced by the patient's own pulmonary valve, which is replaced with a homograft.
- Porcine heterograft (or xenograft) valves.
- Bovine pericardial valves.

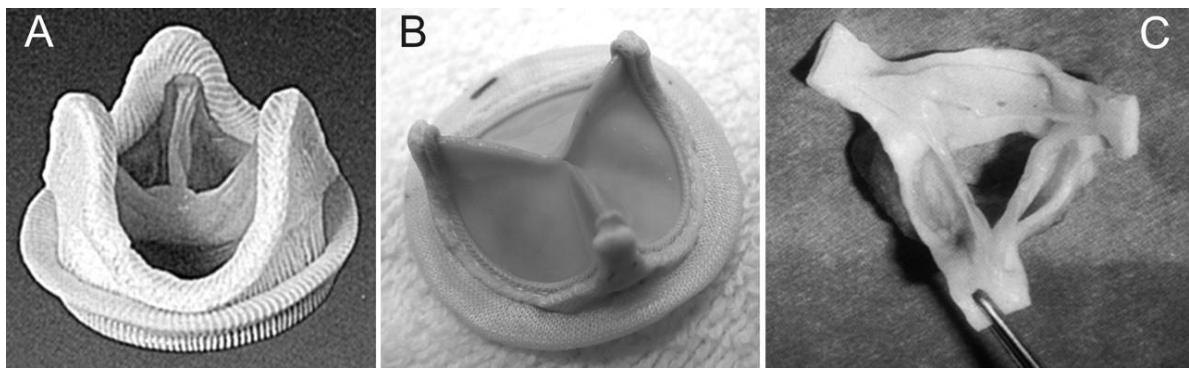


Figure 1.12 - Porcine (A), Bovine (B) and Homologous (C) aortic valves¹⁸

Autografts would be the best choice, followed by homografts.¹⁹ However, there is no abundance of material to perform these types of substitution, thus xenografts are more common.

Xenograft valves can be distinguished in stented and stentless. The stented bioprostheses are mounted on a plastic or metallic stent, covered with polymeric tissues. The stentless ones are directly sutured with the native aortic wall.

The main limit of biological valves is their durability: they can undergo ‘wear and tear’ and consequent degeneration, reducing their live after implantation to 10-15 years.¹⁵

1.4. The aorta

1.4.1. Anatomy and histology

There are three types of arterial vascular systems.

- Elastic arteries include the aorta, carotid artery, brachiocephalic trunk, pulmonary arteries and subclavian artery.
- Muscular arteries are the distributing branches.
- Arterioles are the terminal branches.²⁰

The aorta is the largest vessel in the body. It starts from the left ventricle and transports oxygen-rich blood to the organs. It rises from the heart in antero-cranial direction, then descends in postero-caudal and caudal direction and finally terminates bifurcating into the right and left iliac arteries. It can be divided in six segments²¹:

- the aortic root (light blue in Figure 1.13),
- the sino-tubular junction (green in Figure 1.13),
- the ascending aorta (yellow in Figure 1.13),
- the aortic arch (dark blue in Figure 1.13),
- the isthmus and descending thoracic aorta (red in Figure 1.13),
- the abdominal aorta (pink in Figure 1.13).



Figure 1.13 - Aorta anatomy

The aortic wall is composed of three layers: the tunica intima (or interna), the tunica media and the tunica adventitia (or externa).

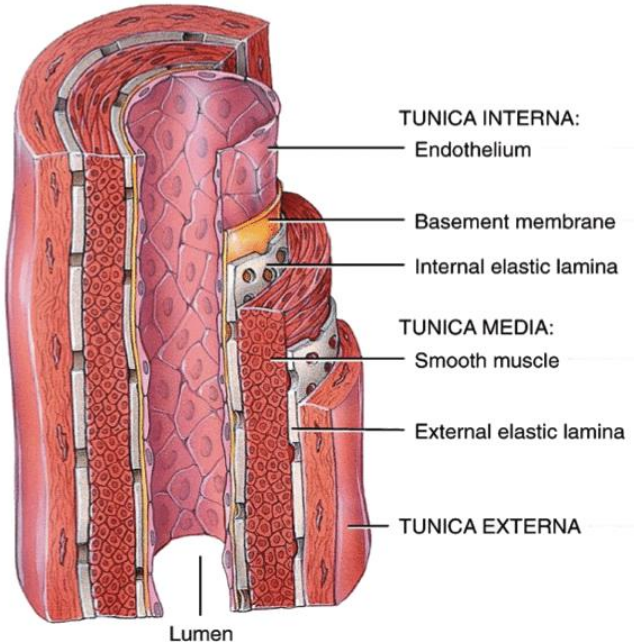


Figure 1.14 - Elastic artery structure²²

The tunica intima

The intima is the inner layer of the aortic wall: it is in contact with the blood. It is made of a non-thrombogenic layer of endothelial cells, contained in an extracellular matrix. The basal lamina (or basement membrane) provides structural support to the wall. Although the intima is very thin, and its mechanical properties do not influence significantly the stiffness of the artery wall in healthy young humans, with ageing the myointimal cells contained in the intima ECM tend to accumulate lipids and increase their thickness. Even in the case of pathological conditions the intima could become thicker and stiffer.²¹ The intima and the media are separated by the internal elastic lamina.

The tunica media

The tunica media is the thickest layer of the aortic wall and it contains many elastic fibers, smooth muscle cells and collagen fibers.²³ These cells and proteins are immersed in the ground substance, containing proteoglycans. The fibers are organized in concentric layers called lamellae, separated by fenestrated sheets of elastin. The collagen fibers are mostly aligned along the circumferential direction and the media determines the mechanical properties of the whole artery wall.²¹ The media and the adventitia are separated by the external elastic lamina.

The tunica adventitia

The tunica adventitia includes collagen and elastic fibers, fibroblast and mast cells. The vasa vasorum, vessels which supply blood to the aortic wall, are contained in the connective tissue which surrounds

the adventitia. The collagen fibers are oriented in the longitudinal direction and remain slack at low pressure, straightening as the pressure increases.²¹

1.4.2. Diseases

Cardiovascular diseases alter the blood flow as a consequence of an obstruction of the lumen, pathological alterations which lead to a decrease of the lumen radius or a contraction of the vessel.¹³

Atherosclerosis

Arteriosclerosis literally means ‘arteries hardening’. This disease comprises various conditions, the most common of which is the atherosclerosis. The atherosclerosis mainly affects the tunica intima of elastic arteries and can advance to the tunica media. The atheroma is a plaque with a lipidic core, a fibrous external cap and various cell types such as macrophages, platelets and fibroblasts. The plaques can spread and increase in number up to cover large parts of an artery, occluding the lumen and altering blood flow. In case of ulceration a thrombus may occur. Increasing their dimensions, plaques tend to invade the tunica media and lead to consequent hemorrhage.

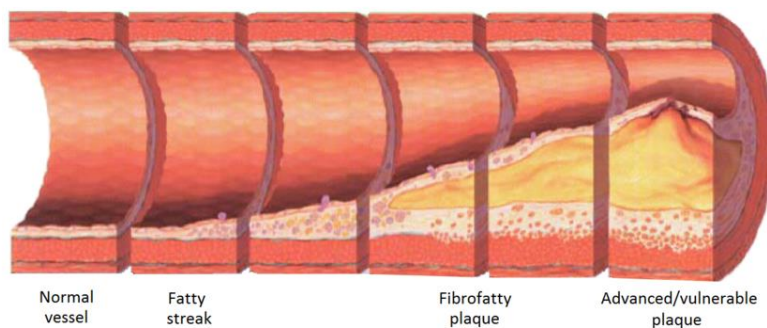


Figure 1.15 - Stages of atherosclerosis

Aortic dissection

The aortic dissection is an interruption of the tunica intima that causes blood entering the tunica media. A dissection is considered acute if the clinical presentation follows the symptom after less than two weeks; otherwise it is chronic.²⁴

The aortic dissection can be classified with various methods considering its clinical importance and the regions involved.

- Stanford aorta dissection type A involves the ascending aorta, while type B involves any other region.
- DeBakey type I dissection involves a tear in ascending aorta complicated by dissections in ascending aorta, aortic arc and descending aorta, while type II consider complications limited to the ascending aorta. DeBakey Type III aortic dissection involves a tear in descending aorta complicated by dissection of descending thoracic aorta (type IIIa) or descending thoracic and abdominal aorta (type IIIb).²⁴

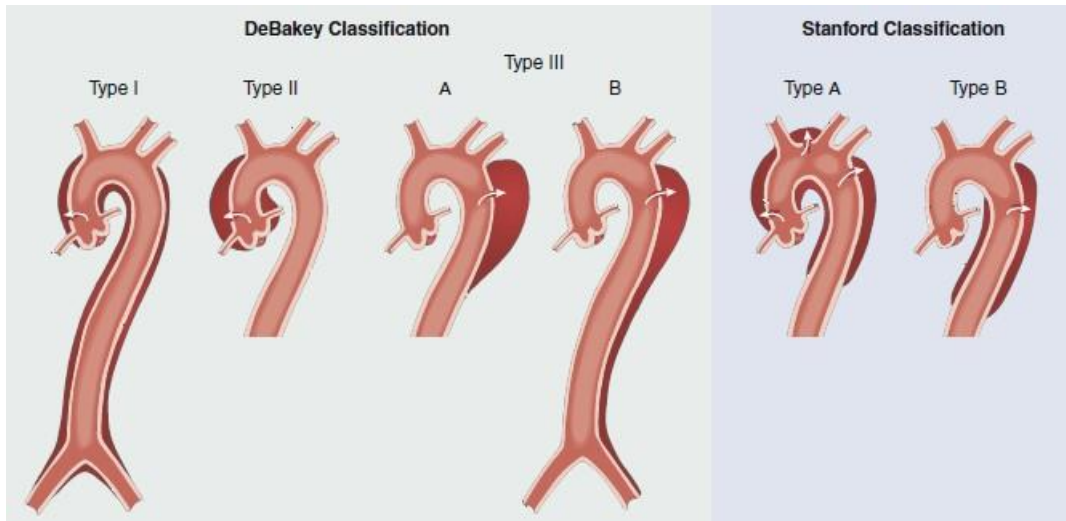


Figure 1.16 - Aortic dissection classifications²⁴

Aneurism

Aneurism is an anomalous dilatation of a vessel due to a weakening of the wall. It can occur in different shapes and is classified according to its anatomy:

- a saccular aneurism is a sac-like wide dilatation of a vessel portion;
- a fusiform aneurism involves the whole vessel circumference.¹³

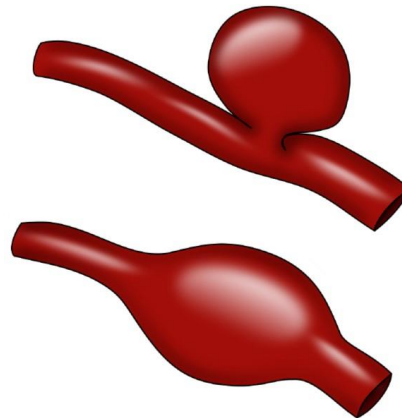


Figure 1.17 - Saccular and fusiform aneurism²⁵

A ‘true’ aortic aneurism involves intima, media and adventitia, while pseudo-aneurisms do not interest all three aortic wall layers. Both types can be caused by atherosclerosis.²⁴

1.4.3. Aorta as a biomaterial

As the wall stiffness is invariably attenuated with an aneurism or a dissection, it is usually treated by replacement with a tubular prosthesis.²⁶

For the reconstruction of large arteries, usually synthetic grafts made of expanded PTFE or Dacron are used. However, for the reconstruction of small caliber vessels (less than 6mm), these materials are not suitable because of their thrombosis risks and a long term antithrombogenic treatment is compulsory.²⁷

For small caliber vessels the best choice would be autografts, but their harvesting involves complicated surgical procedures with resulting enhancing of the risks for the patients.²⁸ The suitable vessels for the substitution should be long enough and have few branches, but there are few candidates with these characteristics in the human and animal vascular systems. Thus, decellularized aorta has been investigated for vascular grafts design.^{27,29,30} The tissue can be decellularized both with mechanical (e.g. high hydrostatic pressure) or chemical (e.g. sodium dodecyl sulphate treatment) methods.²⁹

The aorta has an appropriate length for small caliber vessels replacement, but it is too thick and have too many branches. Tubular prostheses have been designed by peeling of thin sheets, decellularization and production of tubular shaped grafts.²⁷

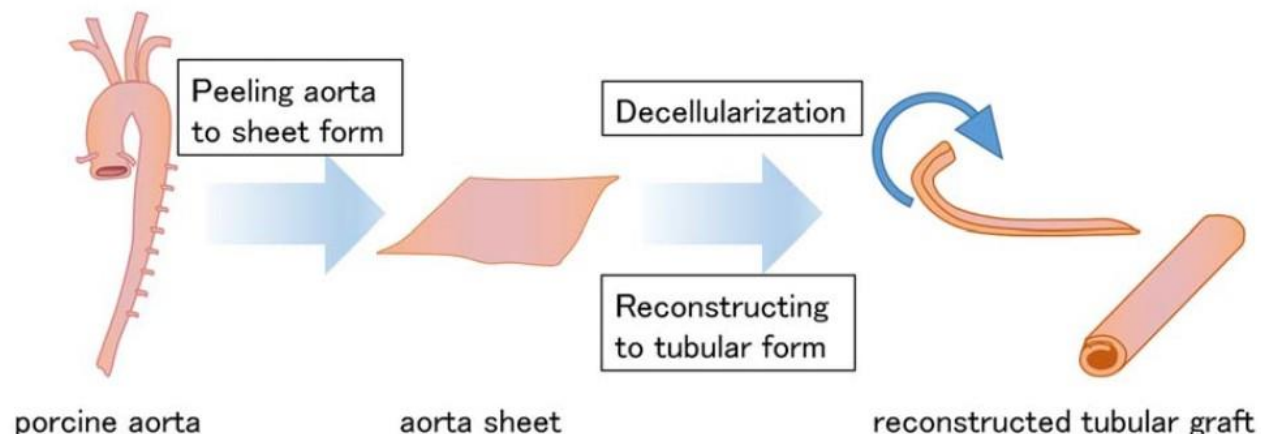


Figure 1.18 - Decellularized tubular graft design from aorta sheets²⁷

Other applications are alternative hemodialysis vascular accesses and scaffolds for tissue engineering of vascular grafts.³¹

1.5. Treatments

As told in the previous paragraphs, the materials used for cardiac bioprostheses design are rich in connective tissue and the collagen is their main component. The main type of collagenous tissues used on this purpose are porcine aortic valve and bovine pericardium. The collagen fibers contained in these tissues are linked by chemical bonds, hydrogen bonds and water-bridged cross-links.

The tissue must be treated before implantation to eliminate its antigenic properties and to arrest its deterioration. The goal is to obtain a non-immunogenic tissue that will degrade in a time longer than the recipient's life, without a significant decrease of the mechanical properties of the tissue.

Treatments usually have the aim of creating new bonds in collagen structure obtaining a strong but non-viable material for the design of bioprostheses.¹⁹ There are chemical and physical methods; the

tissues tested in this thesis were treated with two different chemical agents: glutaraldehyde (GLU) and acid-free glyoxal (GAF).

1.5.1. Glutaraldehyde

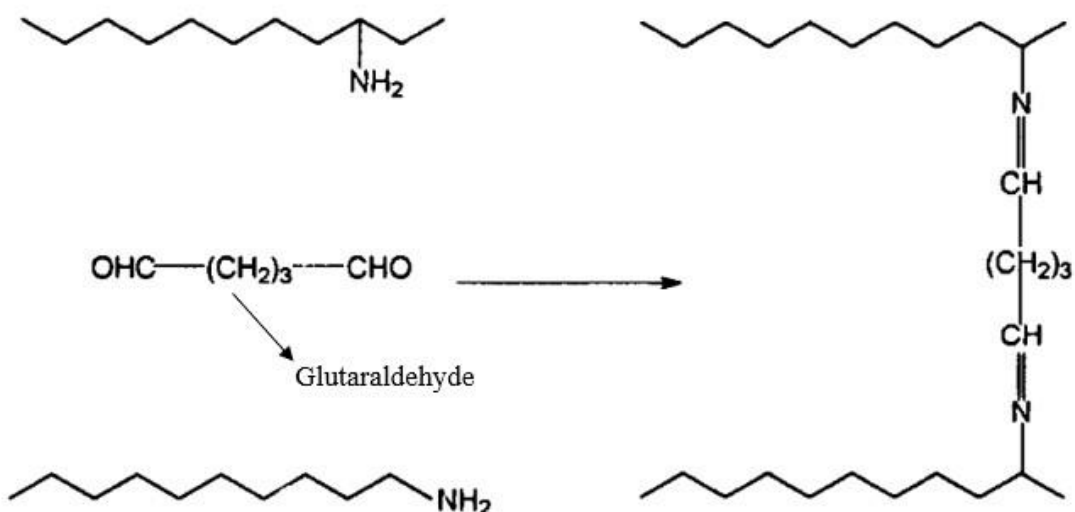


Figure 1.19 - Glutaraldehyde reaction with collagen¹⁹

Glutaraldehyde is a bifunctional molecule composed by a five-carbon chain with an aldehyde at each end. It is the standard agent for collagenous tissues treatments, and it is easily available and inexpensive.

There are several sites of possible chemical reaction in the collagen structure, the main of which are pendant groups like acids (COOH), hydroxyls (OH) and amines (NH₂). The aldehydes can interact with the amines in the collagen structure and form chemical bounds with a collagen molecule at each end of the GLU chain (cross-linking).

Calcification

Calcification is one of the main causes of cardiac bioprostheses failure. The reaction involves non-viable cells and their membrane-associated phosphorus. Normally, a viable cell has a concentration of calcium 1000 to 100000 times lower than the extracellular fluid; a glutaraldehyde-treated cell cannot expulse the calcium in excess, causing the calcification. Moreover, glutaraldehyde stabilizes phosphorous structures in the treated tissue, thus enhancing the calcification.³² This pushed several researchers to search alternative methods for collagenous tissue treatment but none of these has been considered superior to the glutaraldehyde so far.³³

1.5.2. Acid-free glyoxal

Glyoxal is one of the alternative chemical agents which have been proposed to replace the glutaraldehyde for collagenous tissues treatment. It is an organic molecule with two aldehydes, and it is the smallest of dialdehydes. Its chemical formula is OCHCHO. Although glyoxal is not toxic and not classifiable as a human carcinogen, it irritates skin and eyes. Since commercial available glyoxal

is acid, an acid-free form of glyoxal has been devised and investigated by the Department of Medical Sciences (University of Turin) and it has been established that it can be a valid fixative for collagenous tissues, producing a preservation of macro-molecular properties similar to that obtained with standard methods.³⁴ GAF produces a non-viable tissue like the one obtained with the standard process, without enhancing the calcification phenomena; thus, it has been taken in consideration as a possible substitute for the glutaraldehyde.

However, an essential requirement in cardiac bioprostheses design is the mechanical performance of the starting material, and each fixation treatment may compromise the tissue structure, consequently deteriorating its mechanical properties. Mechanical properties of GAF-treated tissue remain to be clarified, which leads to the purpose of this thesis.

1.6. Mechanical characterization

Mechanical biaxial characterization of soft biological tissue is very challenging. Among the main difficulties there are the usually small dimensions of the specimens, the specimen-to-specimen variability, time dependent results caused by biological degradation, gripping difficulties and significative influence of the gripping system on the results. Nonetheless, biaxial testing is the only way to obtain a 3D characterization of the tissue, which is not possible with uniaxial tests.^{35,36}

Biological tissues have been studied several times and many attempts have been made to obtain a constitutive model. The mechanical properties are strongly influenced by the inner structure of the ECM. The material is anisotropic, and the material axes usually correspond to the preferred and cross-preferred directions of the collagen fibers. It has been demonstrated that biological tissues are stiffer in the collagen fibers direction.^{37,38} There are several ways to determine the material axes but none of these is lacking in difficulties and inaccuracies. One of the main methods is the small angle light scattering (SALS)^{37,39}, though mechanical methods have also been tested.

Mechanical tests for biaxial characterization can be conducted both in a displacement-controlled or load-controlled manner. The latter allows to apply a test which simulates the *in vivo* nominal stresses.³⁹ The test is usually composed of an equibiaxial preconditioning followed by a series of cycles with variable rate between the displacements (or loads) along the system axes.³⁸⁻⁴⁰

Deformation should be measured in the central region of the specimen to avoid tethering effects and the measurements must be optical to avoid mechanical interference.³⁸

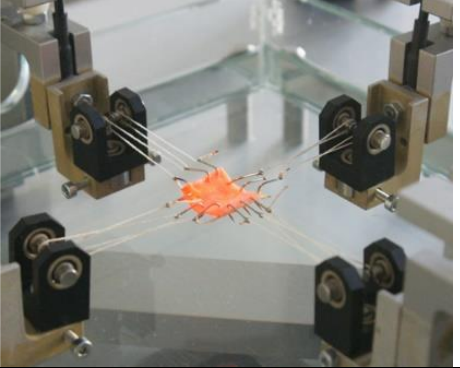
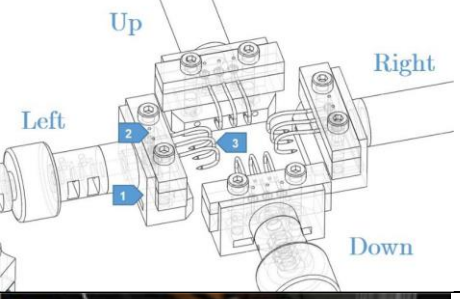
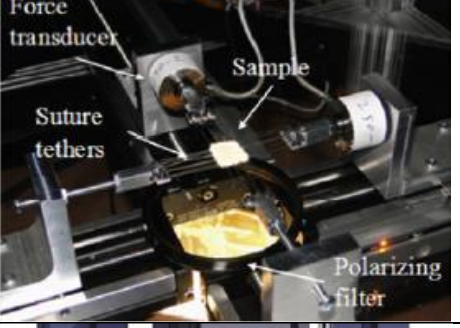
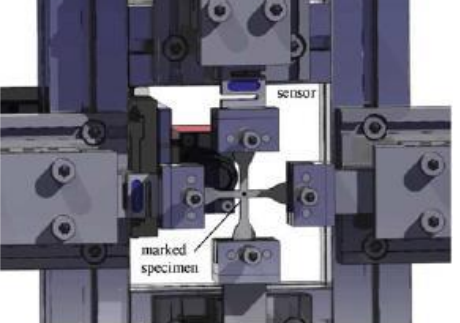
Usually, a four-markers matrix is placed in the central region of the specimen. Various types of markers have been used before, in both paint and physical forms:

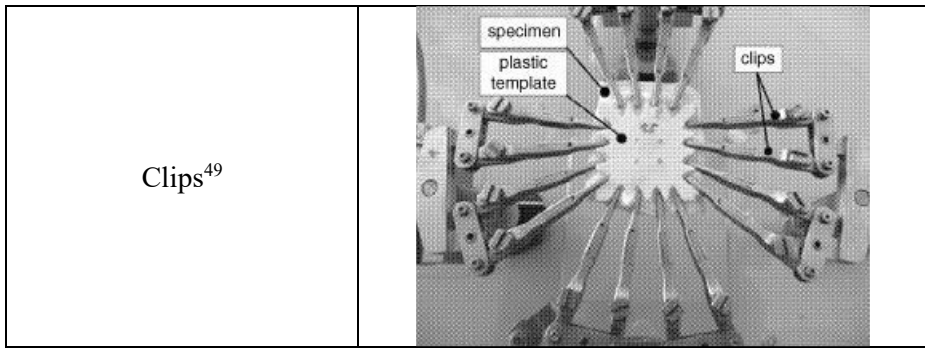
- graphite markers glued with cyanoacrylate adhesive^{37,39};
- India ink⁴¹;

- enamel paint⁴²;
- commercial lacquer⁴³;
- acrylic paint⁴³;
- physical marker glued with medical spray band⁴³;
- waterproof dyeing⁴⁴.

Several attachment systems have been used for soft tissues mechanical biaxial testing, the main types are listed in the following table.

Table 1.1 - Gripping systems for soft tissues biaxial characterization

Hooks and suture ⁴⁵	
Interlocked hooks ⁴⁶	
Suture loops ⁴⁷	
Clamp tensile grips ⁴⁸	



For the study described in this thesis, thin threads were tied up with hooks inserted along each edge of square-shaped specimens. With such a grip technique, the specimen can shear freely and undergo lateral deformation. The whole test should be performed in physiological saline at controlled 7.4 pH at room temperature or at 37°C.³⁸ To correlate the mechanical response with the ECM matrix structure, preferred and cross-preferred collagen fibers directions should be aligned with the test system axes. The load can be distributed along the edges of the specimen in an equal manner using pulleys-provided gripping systems.⁵⁰

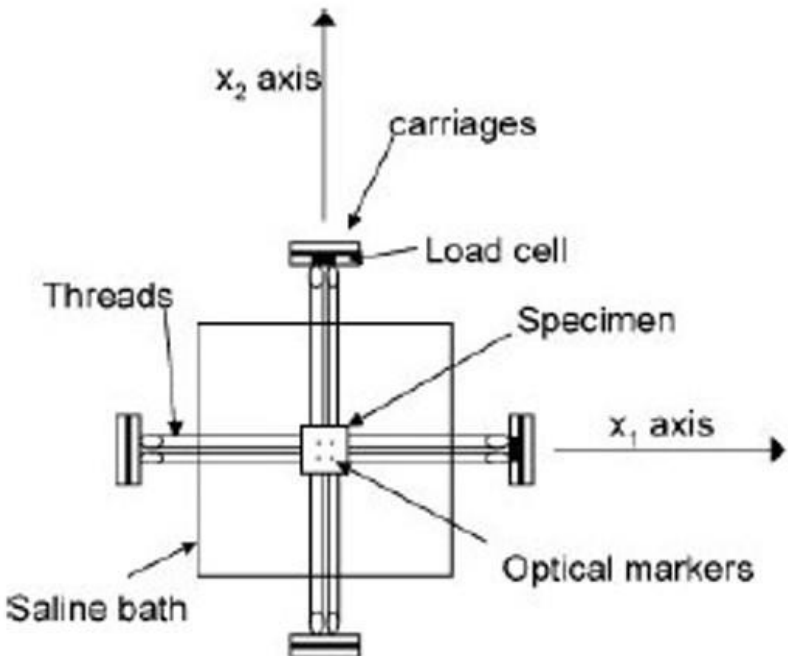


Figure 1.20 - Soft biological tissues biaxial mechanical testing³⁸

1.6.1. Control loop tuning

A control system is a mechanism which measures and controls a process. In mechanical tests the output can be a displacement, a strain, a stress or a load. In any case, a control loop is needed to correct the differences between the desired output and the process variable. In order to do this, open loop or closed loop control systems can be used. In the first case, the output only depends on the input

and no other feedback is considered. A closed loop relies on a feedback and adjust the output as needed.



Figure 1.21 - Open (left) and closed (right) loop systems

A proportional-integrate-derivate (PID) controller calculates the error between the process variable and the setpoint, the integral of previous errors and the rate of change of the error itself and compute a corrective action using a weighted sum of these terms. The weights are called tuning parameters and the tuning is the process of selecting their values. A close controlled loop tuning has been applied for the biaxial testing load-controlled protocol, which is detailed below.

2. Materials and methods

2.1. Specimens preparation

Samples were cut in rectangular shape with edges parallel to the apex-base and circumferential directions for the pericardium and to longitudinal and circumferential directions for the aorta. The samples were used to produce specimens for biaxial mechanical characterization.

Table 2.1 - Number of load-control tested specimens

Pericardium			Aorta	
Fresh	GLU	GAF	GLU	GAF
3	1	1	1	1

Table 2.2 - Number of displacement-control tested specimens

Pericardium		Aorta	
GLU	GAF	GLU	GAF
4	4	4	4

For the biaxial test, $15 \times 15 \text{ mm}^2$ square shaped specimens were used, with the edges parallel to the directions mentioned above. These specimens underwent thickness measurement and mechanical test. Before the latter, four markers were drawn in the central region of the square with a permanent marker for optical strain computation. Since the specimens are square shaped, a suture thread was inserted in each specimen along the circumferential edge to take note of the directions.



Figure 2.1 - GAF-treated pericardium specimen

2.2. Thickness measurement

2.2.1. CNC controlled scanning probe

Thickness of each specimen was measured with the CNC machine Roland MODELA MDX-40A. It is a milling and cutting machine, but it can be used as a 3D scanner with the Roland ZSC-1 3D scanning sensor unit.



Figure 2.2 – Roland MODELA MDX-40A (left) and scanning sensor unit (right)

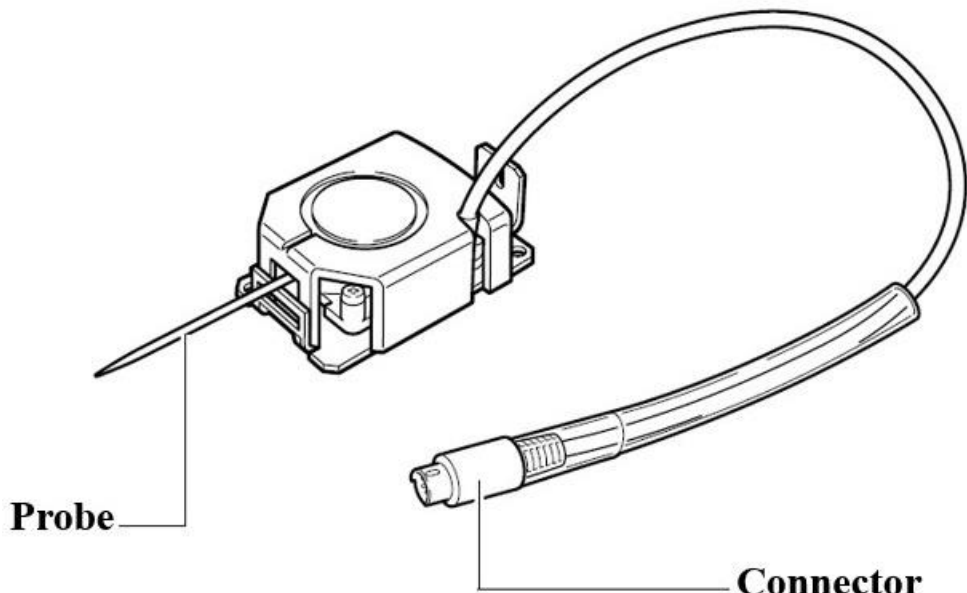


Figure 2.3 - Roland ZSC-1 3D scanning sensor unit⁵¹

The sensor can detect the 3D shape of the object of interest with a scan controlled by the Dr. PICZA3 software. The orange quadrilateral in Figure 2.4 represents width and depth of the scanning area. The buttons below can be used to verify or set the area, move it, zoom it and go back to the default view. The scanning area can be modified either typing the upper-right and lower-left vertices coordinates or dragging the red squares in the vertices of the orange quadrilateral.

To set the height of the scan zone is possible to specify a minimum and a maximum quote. The first one can be typed in the specific box, the second can be detected by the scanning probe selecting a point in the scanning area in which the maximum height of the object is supposed to be. Finally, a pitch for the scan can be set in both width and depth directions.

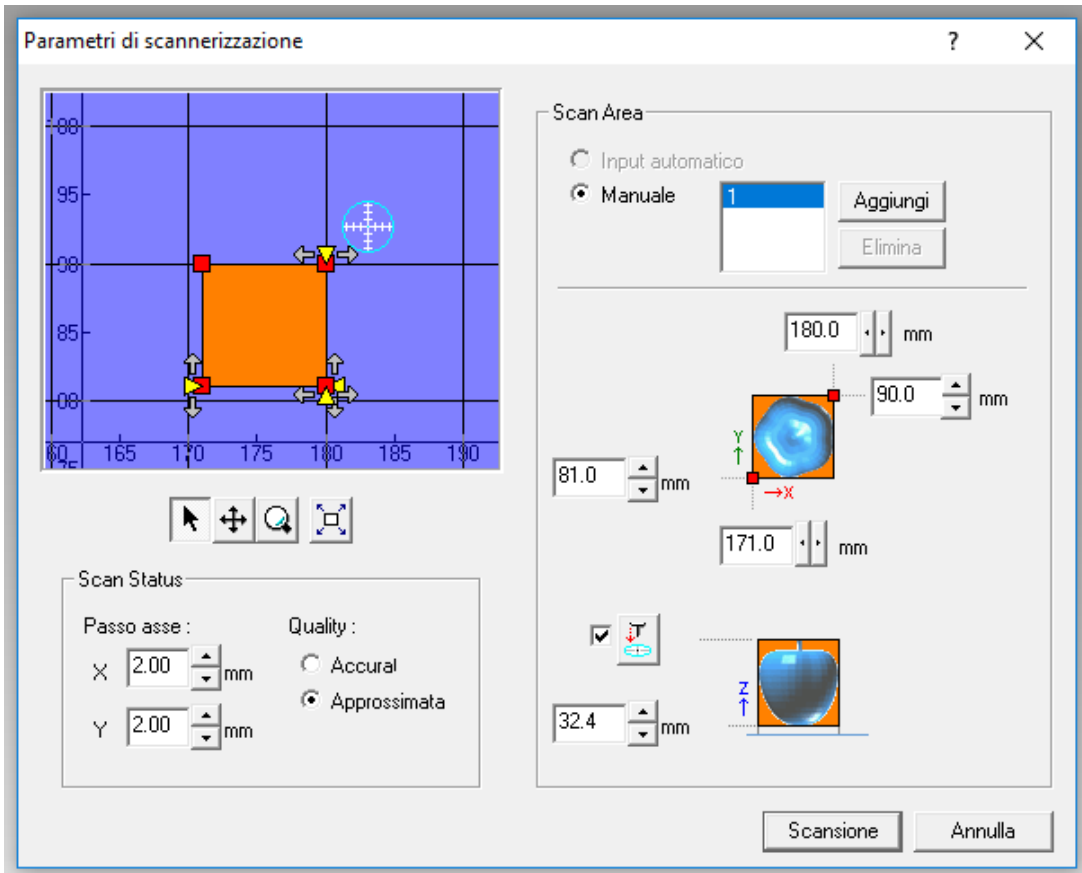


Figure 2.4 - Dr. PICZA3 user interface

The scan data can be exported in various format, in this case a group of point was exported, with the spatial coordinates of each point detected by the tool. The height values were used for thickness calculation, which will be detailed in paragraph 2.2.3.

2.2.2. Sample holder

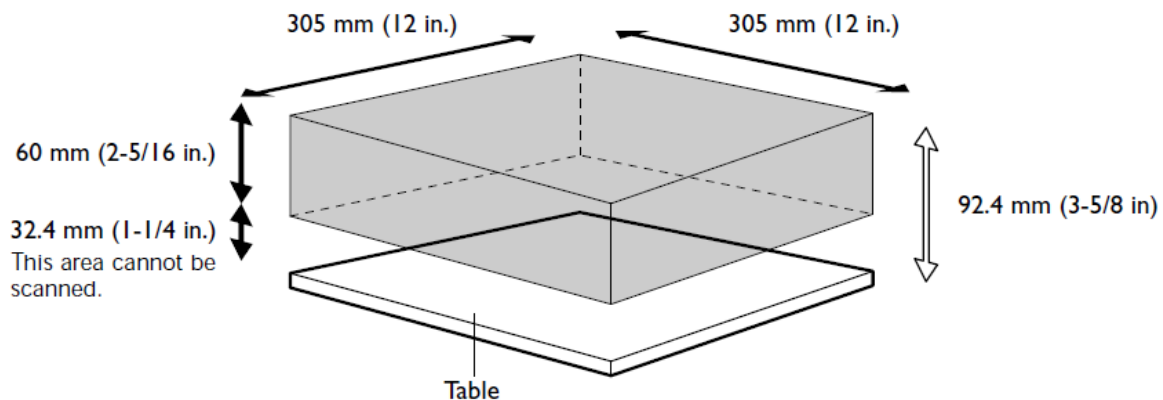


Figure 2.5 - ZSC-1 scanning volume⁵¹

Since the scanning volume has a minimum height of 32.4 mm and no object can be detected below this value, the design of a specific holder has been compulsory for the thickness measurement. The holder was designed using SolidWorks and 3D-printed using a Stratasys UPrint SE Plus desktop 3D printer. It is a $30 \times 37 \times 30$ mm³ parallelepiped with a step on its upper surface, which is a 15×15 mm²

square-based parallelepiped with 10 mm of height. The sample was placed on the top of the step; therefore, it was at 40 mm of height, which is detectable by the CNC machine.

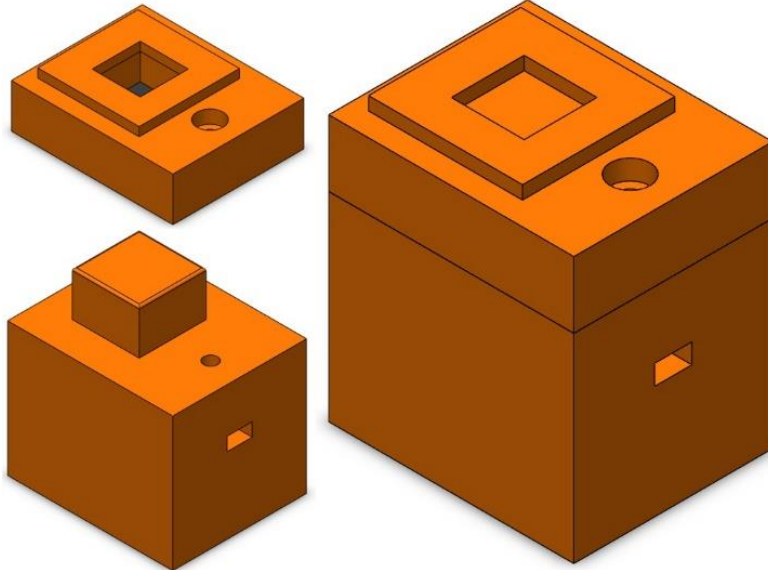


Figure 2.6 - Specimen holder: parts and assembly

To avoid unexpected translations of the sample during the measurement, a cover was designed. It was placed on the holder and fixed with a screw. It has an $11 \times 11 \text{ mm}^2$ window and a step on its surface. The window allows the thickness measurement in the central region of the specimen and the step is useful to determine the maximum scanning height as described above. This system allowed to calculate the thickness of the sample as the difference between the quote measured with and without the specimens.

2.2.3. Measure procedure

The thickness was measured in an $8 \times 8 \text{ mm}^2$ 25-points matrix in the center of the specimen. First, the height of the holder (Z_0^*) was measured as the mean height in the 25 points detected in a scan with no specimens on the holder. Next, the specimen was placed on the holder and the same scan has been performed, measuring the total quote of the specimen-holder ensemble (Z^*). The thickness of each specimen was calculated as the difference between Z^* and Z_0^* .

$$T_i^* = Z_i^* - Z_0^*$$

After few measurements, it was established that the scanning probe used to penetrate the tissue during the scan, underestimating the thickness and potentially damaging the tissues. To avoid it, a square shaped plastic leaf was placed on the specimens before the measurement, as shown in Figure 2.7. Thus, the new calculation of the thickness was the difference between the total holder, specimen and leaf quote (Z) and the quote without the specimen (Z_0).

$$T_i = Z_i - Z_0$$



Figure 2.7 - Thickness measurement process

2.2.4. Thickness values

The thickness of all specimens is shown in the following table. The specimens have been divided in two groups according to the two different protocols described below.

Table 2.3 - Specimens thickness

	Specimen	Thickness [mm]
Load-controlled protocol	GAF Pericardium	0.46
	GLU Pericardium	0.81
	GAF Aorta	2.45
	GLU Aorta	2.14
	Fresh Pericardium 1	0.46
	Fresh Pericardium 2	0.72
	Fresh Pericardium 3	0.68
Displacement-controlled protocol	GAF Pericardium 1	0.39
	GAF Pericardium 2	0.71
	GAF Pericardium 3	0.51
	GAF Pericardium 4	0.34
	GLU Pericardium 1	0.50
	GLU Pericardium 2	0.45
	GLU Pericardium 3	0.73
	GLU Pericardium 4	0.93
	GAF Aorta 1	2.26
	GAF Aorta 2	2.33
	GAF Aorta 3	3.08
	GAF Aorta 4	2.83
	GLU Aorta 1	2.90
	GLU Aorta 2	2.46
	GLU Aorta 3	3.00
	GLU Aorta 4	2.96

2.3. Biaxial mechanical testing

2.3.1. System description

Mechanical tests were performed with ElectroForce LM1 TestBench Test Instrument. It is a specifically developed system for the characterization of soft tissues and can be used for both uniaxial and biaxial characterization. It is composed of a perforated table (reaction base) on which four movers

can be screwed in different positions. Two 225 N load cells, a bath assembly for wet temperature-controlled tests and different grip fixtures are also provided.

For biaxial mechanical test the four motor have been placed as shown in Figure 2.8, one at each side of the bath. Motors 1 and 2 are aligned to motors 3 and 4 respectively.

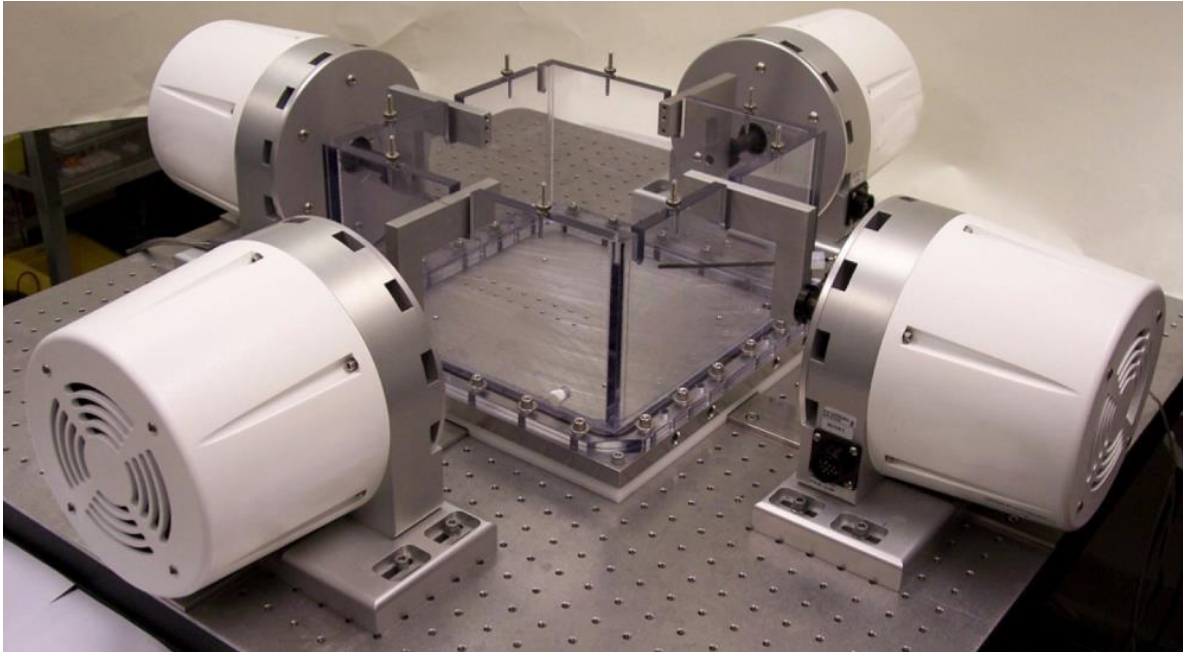


Figure 2.8 - Powerheads placement⁵²

Each motor has a stroke which goes from -6.25 mm (toward the center of the bath) to +6.25 mm (toward the power head).

Two of the grip fixtures shown in Figure 2.9 were mounted together with the load cells and screwed on the brackets of movers 1 and 2, the other two are screwed on the brackets of movers 3 and 4, without any load cell. In this manner, each of the two axes has a motor with a load cell and the other one without it.

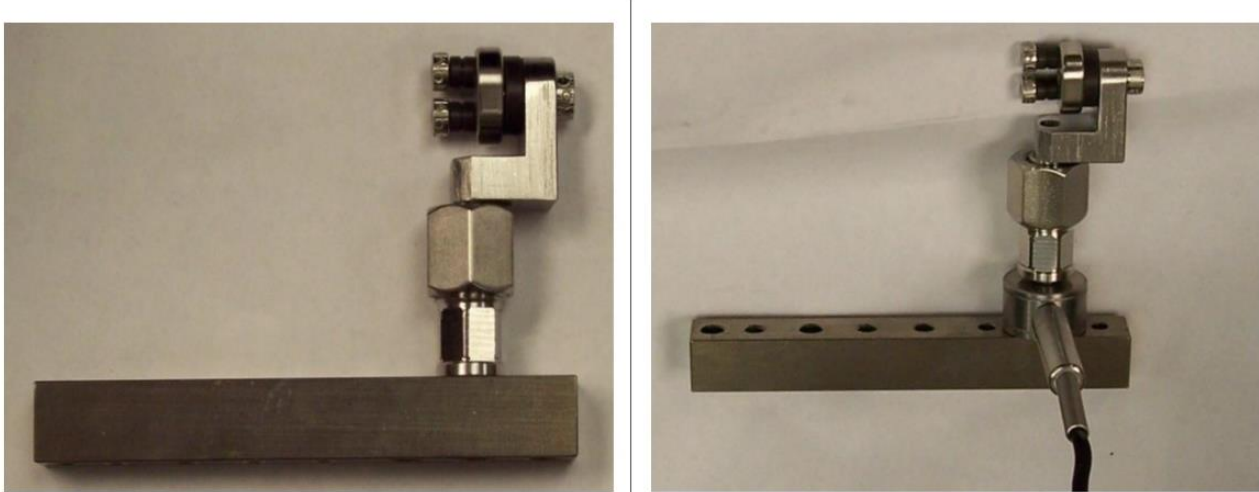


Figure 2.9 - Biaxial characterization grip fixtures, with (right) and without (left) a load cell⁵²

In order to achieve the maximum stroke, all movers were moved toward the middle of the table using a 3D-printed spacer to set their positions in a reproducible manner. The spacer is an $80 \times 80\text{mm}^2$ square

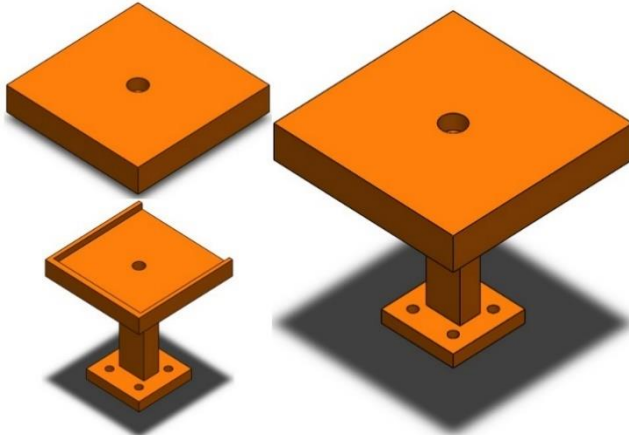


Figure 2.10 - Spacer and support

screwed on a support, which is in turn fixed in the center of the bottom of the bath. This allows to place the motors in the same positions every time after moving them and to ensure the same distance of each motor from the center of the system. The distance between each mover was decided according to the dimensions of the specimens and their mounting technique, described below. The support designed for the spacer was also devised to facilitate the specimen placement in the test bench.

During the positioning of the motors, their brackets were in the -6 mm position, so that a 12.25 mm stroke per motor (24.5 mm per axis) was guaranteed for the test. Each test started with all motors having a -6 mm displacement, in order to facilitate sample mounting.

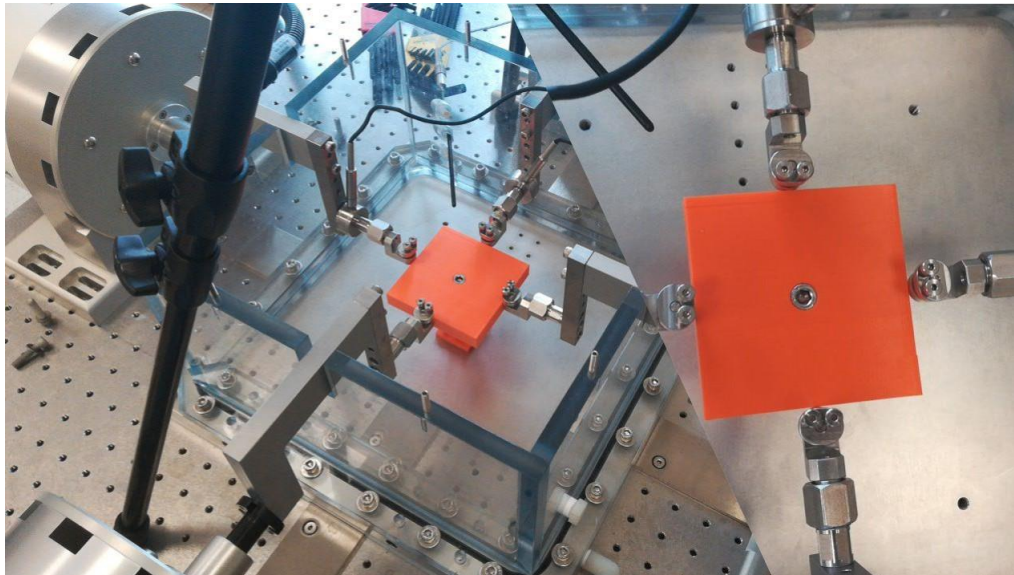


Figure 2.11 - Motors placement for biaxial mechanical tests

2.3.2. Specimen mounting

As explained in paragraph 1.6, for biaxial tests, a soft tissue should be gripped using thin threads to achieve the optimal gripping technique and limit tethering effects as much as possible. In this case fishing hooks and line were used to build the gripping tools. The insertion of the hooks was carried out using a specially designed insertion fixture provided together with the other ElectroForce LM1 TestBench Test Instrument tools.

Initially, the specimen was placed on the bottom part of the fixture, centering it on the step. Then, the top part of the fixture was placed on it. For the grip, eight combination of one string with a hook tied on each extremity were used (16 hooks and 8 strings in total). 4 hooks were put through each edge of the specimens resulting in 2 bent wires per edge. The specimen needed to stay wet, so the whole process was performed into a case full of water.

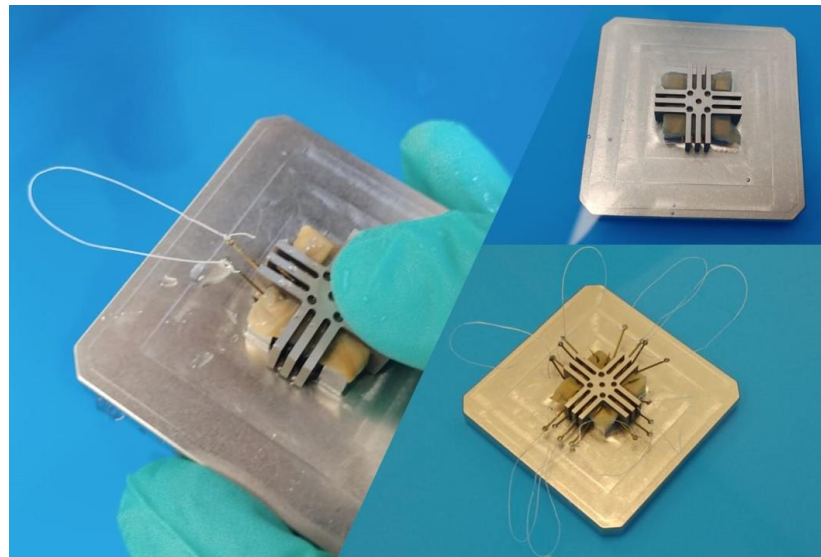


Figure 2.12 - Hooks insertion

The external hooks of each edge had a mutual distance of 8 mm, which can be considered the length among which the force is applied. The hooks and string combinations were finally looped around the spokes of the grip fixture and the pulley system ensured that the force was equally distributed along this length during the test.

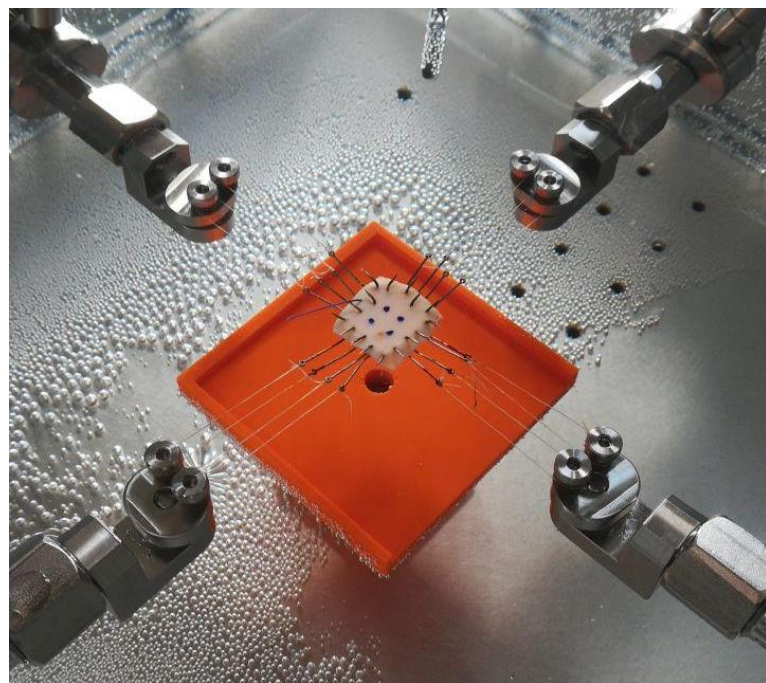


Figure 2.13 - Specimen mounting

2.3.3. WinTest

WinTest is the software which allows to interface ElectroForce instruments with the computer. Motors can be controlled with different strategies, including displacement ('Disp'), 'Load' and displacement difference ('DispDiff'). This last can be used to set a motor movement in order to replicate the displacement of another motor (e.g. with DispDiff1-3=0, motor 3 will reproduce symmetrically the displacement of motor 1).

Different types of waveforms, such as ramps, triangular and sine waves, can be imposed to the motors. It is also possible to perform a block of waveforms, combining different types. Parameters and data from the movers and the load cells (i.e. Disp of each mover and Load of each cell) can be observed directly in the user interface, together with the scope windows. These last are used to represent diagrams of some variables depending on another. In this thesis 'Load vs Time', 'NetDisp vs Time' and 'Load vs NetDisp' were used, being 'NetDisp' the sum of the displacements of two aligned motors (i.e. the displacement applied along a direction of the sample). The temperature of the bath can also be set; for our tests it was set at 37 °C. In WinTest is possible to collect the test data with different sample rates. A 25 Hz sample rate has been used to synchronize the acquisition of machine data and the frame rate of the camera (25 FPS). These data can be finally exported in a std file or in a spreadsheet, which was used for data analysis in MATLAB R2019a.

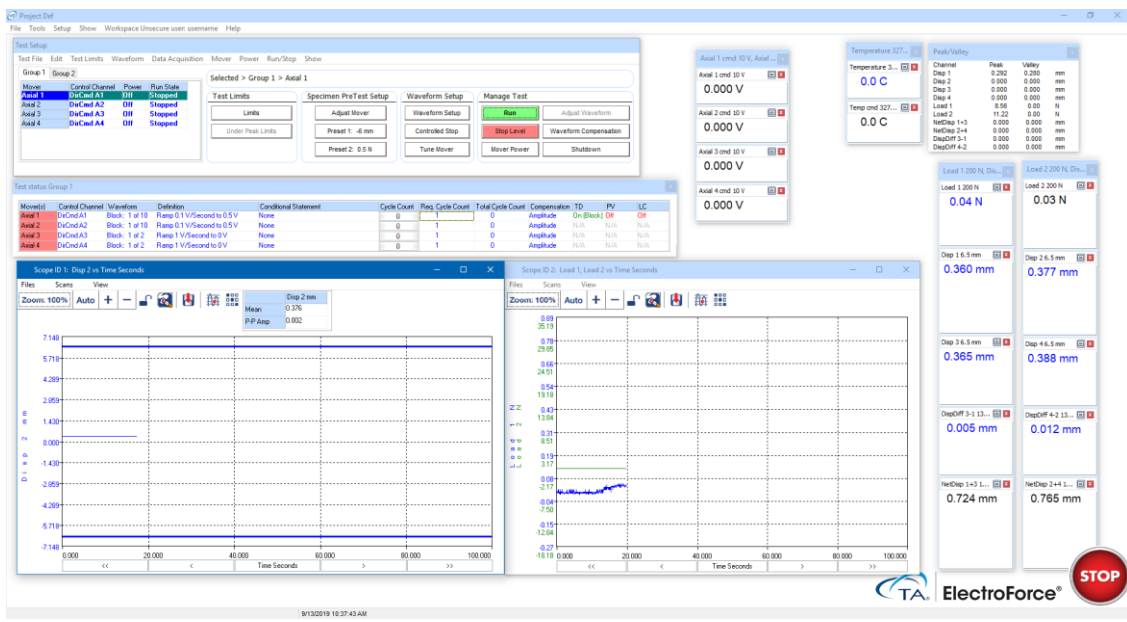


Figure 2.14 - WinTest user interface

In order to simplify the dissertation, the directions along motors 1 (as well as 3) and 2 (as well as 4) will be referred to as axis 1 and axis 2 in the following.

Tuning

An automatic tuning function is available in WinTest. The process is compulsory in order to perform load-controlled tests. A specimen must be mounted in the TestBench and the software can compute

the tuning parameters with a completely automatic routine by testing the sample. A different tuning should be performed for each type of specimen (e.g. one for pericardium and one for aorta).

2.3.4. Load-controlled biaxial protocol

To perform the load-controlled protocol, DispDiff=0 was imposed to motors 3 and 4, so that they symmetrically reproduced the displacements of motors 1 and 2 respectively. The load-controlled protocol was applied at these last with a block of waveforms. It was divided in two phases: the first one consisted in 10 preconditioning cycles of sine waves with maximum amplitude in both directions; the second one was composed of 7 cycles with different ratios between F_1 and F_2 , being these the forces applied along axis 1 and 2 respectively. The peak force reached during the test was set to obtain a maximum stress σ of 0.5 MPa; the value was chosen to double the 250 kPa physiological nominal stress in bioprosthetic heart valves.^{53,54} The stress was calculated as the force divided by the resistant section.

$$\sigma = \frac{F}{T \times L} \left[\frac{N}{mm \times mm} = MPa \right]$$

Being T and L the thickness of the specimen and the length among which the force is applied.

The valley of each wave was equal in force to 0.5 N to keep the specimen in tension throughout the test. The force-controlled test started with a ramp toward 0.5 N; when the value was reached in both directions, 10 cycles from 0.5 N to the maximum force were performed and followed by the 7 cycles described in Table 2.4. All the sine waves were performed with a frequency of approximately 0.03 Hz. Specimens were immersed in water at 37 °C throughout the test.

Table 2.4 - Load-controlled biaxial protocol

	Phase 1		Phase 2					
Cycle	1-10	1	2	3	4	5	6	7
$F_1:F_2$	1:1	10:1	2:1	4/3:1	1:1	1:4/3	1:2	1:10

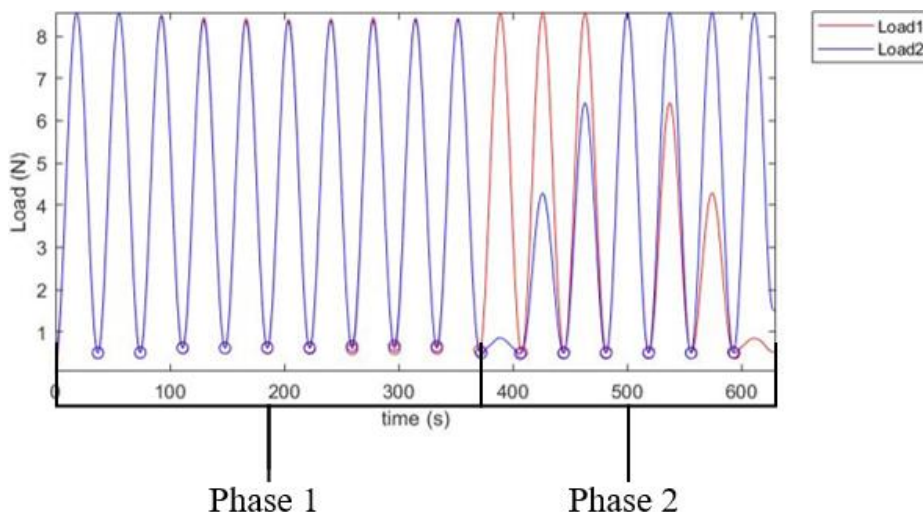


Figure 2.15 - Load-controlled protocol example (filtered data)

For some specimens, in the second phase of the protocol, the peak F_2 in first cycle and F_1 in the last one, would have been lower than 0.5 N, which is the valley in the other cycles. For this reason, the first and last cycle were replaced with a copy of the second and the second-last respectively.

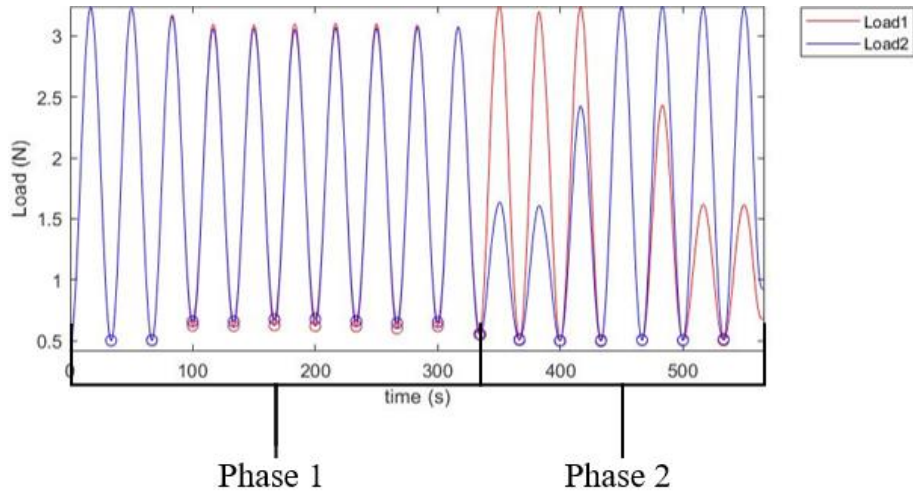


Figure 2.16 - Modified load-controlled protocol example (filtered data)

Load and NetDisp recorded during the test in both directions were exported and the tests were video recorded using Canon DS126201 with Canon macro lens EF 100 mm 1:2.8 USM. The position of the previously drawn markers allowed the calculation of the strain in the central region of each specimen.

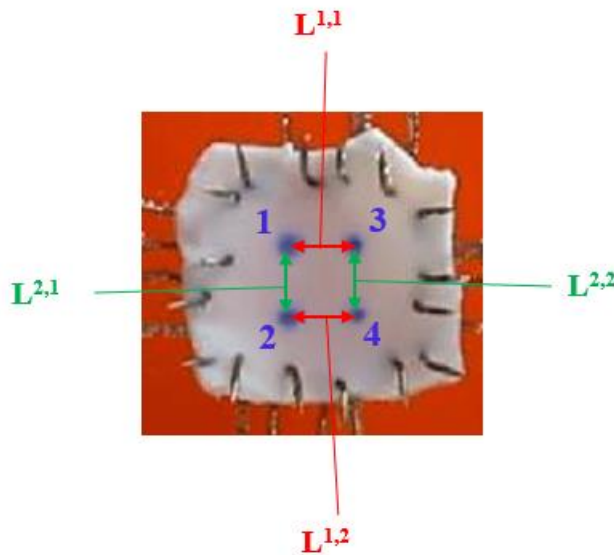


Figure 2.17 - Markers for strain computation

The distance along axis 1 was calculated as the mean distance between the centroids of ROI 1 and 3 and 2 and 4. A similar process was used for axis 2.

$$L^1 = \frac{L^{1,1} + L^{1,2}}{2} [mm]$$

$$L^2 = \frac{L^{2,1} + L^{2,2}}{2} [mm]$$

The strains ε were calculated along each axis with the following equations.

$$\varepsilon^1 = \frac{L^1 - L_0^1}{L_0^1} \left[\frac{\text{mm}}{\text{mm}} \right]$$

$$\varepsilon^2 = \frac{L^2 - L_0^2}{L_0^2} \left[\frac{\text{mm}}{\text{mm}} \right]$$

L_0 is the value of L in the first frame, which corresponds to the test start.

Issues and difficulties

The load-controlled test allowed to determine the correspondence between loads and displacement in the specimens listed in Table 2.1. Initially, a set of specimens was used to perform a tuning for the four types of specimens available:

- GAF-treated aorta;
- GLU-treated aorta;
- GAF treated pericardium;
- GLU treated pericardium.

Like explained above, a tuning should be performed for each type of test and specimen. However, it proved to be specimen-specific, so that a tuning would have been needed for each specimen. Indeed, the force values are different for each specimen depending on the thickness, and the tuning routine is force-dependent. For these reasons, the load-controlled tests performed on the specimens in Table 2.1 were affected by several problems.

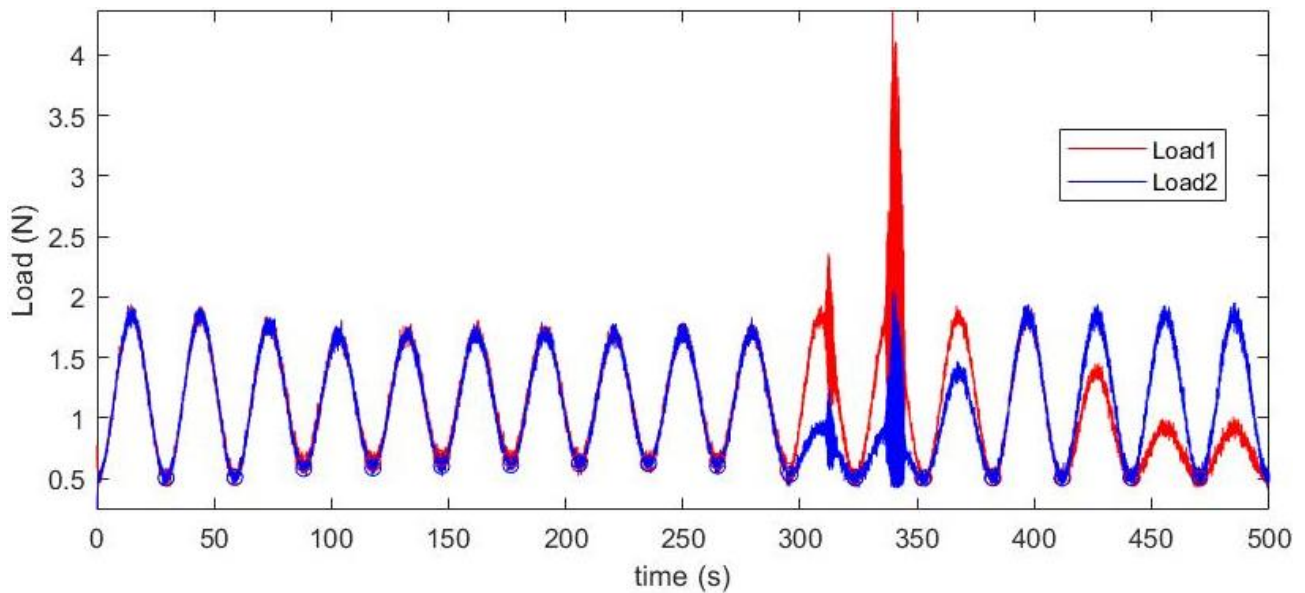


Figure 2.18 - GAF-treated pericardium: Load vs time (raw data)

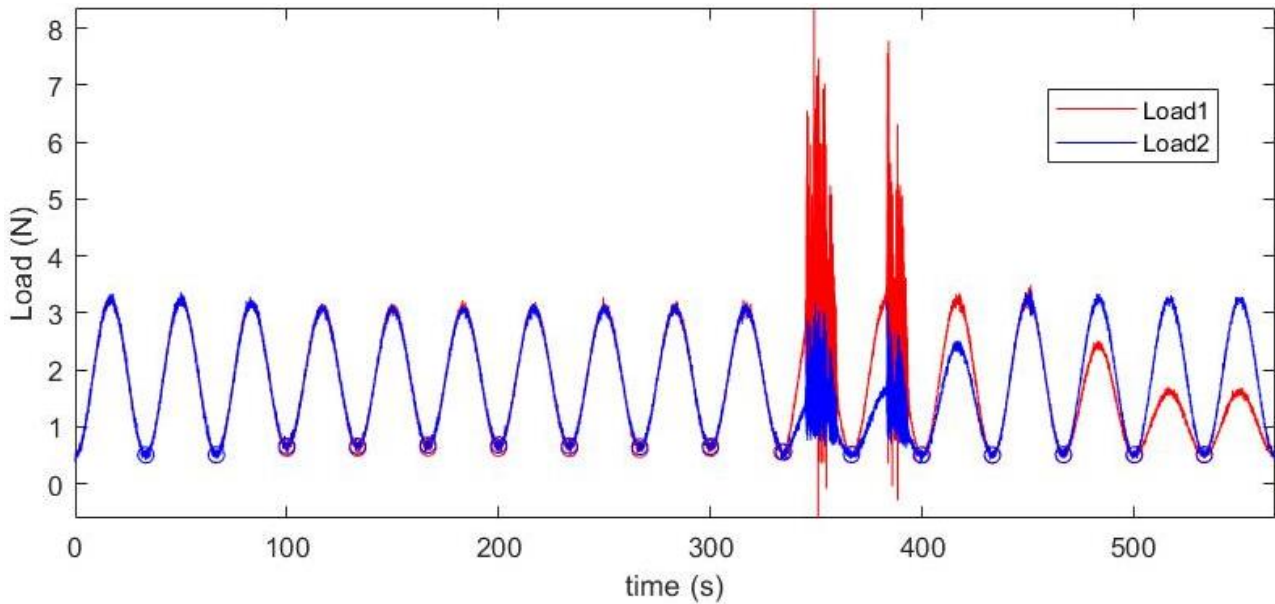


Figure 2.19 - GLU-treated pericardium: Load vs time (raw data)

In both the tests shown in Figure 2.18 and Figure 2.19, massive vibrations can be observed during the first two cycles of the second phase of the protocol. This could be caused by an inappropriate tuning in the axis 2 direction. Indeed, the problem occurs in correspondence of the lowest force peaks of the entire protocol. The control of lowest peaks would have needed a specific tuning in order to avoid issues, which also explains why the pericardium is the most critical tissue, since it has been tested with lower forces.

Moreover, the tuning procedure has been destructive for a few specimens and could have damaged the others, changing their mechanical properties. A specific tuning procedure for each specimen before the tests would therefore not be advisable. For these reasons, a displacement-controlled protocol was devised to avoid tuning and enhance the control accuracy of the tests.

2.3.5. Displacement-controlled protocol

The new protocol was divided in two phases as well as the first one, one equibiaxial and the other with different displacement rates between the axes from cycle to cycle. This time, triangular waves were utilized in order to maintain a constant rate during each cycle. A nominal maximum stress of 0.5 MPa remained the desired value, thus each specimen underwent an initial equibiaxial ramp to discover the displacement corresponding to the force which ensured the desired stress. The stretch rate was set equal to 0.32 mm/s (0.16 mm/s along each axis), so the frequencies of the triangular waves depended on the amplitudes.

Table 2.5 - Displacement-controlled biaxial protocol

Cycle	Phase 1		Phase 2				
	1-10	1	2	3	4	5	
D ₁ :D ₂	1:1	3:1	2:1	1:1	1:2	1:3	

After the first measurements, it was established that a wave maximum amplitude of 2.30 mm for the aorta and 1.00 mm for the pericardium allowed to achieve the desired maximum stress (0.5 MPa) for the most part of the samples. For this reason, it was decided to use the same maximum amplitude for each test. This also allows to perform a repeatable test for each specimen, differently from what happened with load-controlled protocol, which was specimen-specific.

Each test started with the specimen already in tension, so no ramp to initial value was needed. Although the amplitude was equal for all the tests performed on same-tissue samples, the initial value of the displacement in order to obtain a tense status of the sample strongly depended on the specimen mounting (e.g. the distance between its edges and the hooks insertions), which was not easily repeatable. Thus, the block waveform was performed in a relative reference system: each motor covered the desired stroke, regardless of the starting point.

Table 2.6 - Pericardium displacement-controlled protocol

	Cycle	D1/D2	Disp1 [mm]	Disp2 [mm]
Phase 1	1-10	1	1.00	1.00
Phase 2	1	3	1.00	0.33
	2	2	1.00	0.50
	3	1	1.00	1.00
	4	1/2	0.50	1.00
	5	1/3	0.33	1.00

Table 2.7 - Aorta displacement-controlled protocol

	Cycle	D1/D2	Disp1 [mm]	Disp2 [mm]
Phase 1	1-10	1	2.30	2.30
Phase 2	1	3	2.30	0.77
	2	2	2.30	1.15
	3	1	2.30	2.30
	4	1/2	1.15	2.30
	5	1/3	0.77	2.30

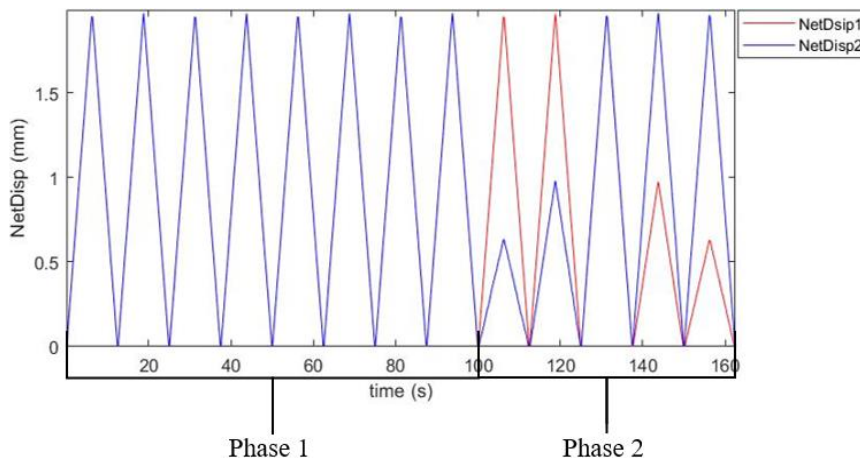


Figure 2.20 - Pericardium displacement-controlled protocol example (raw data)

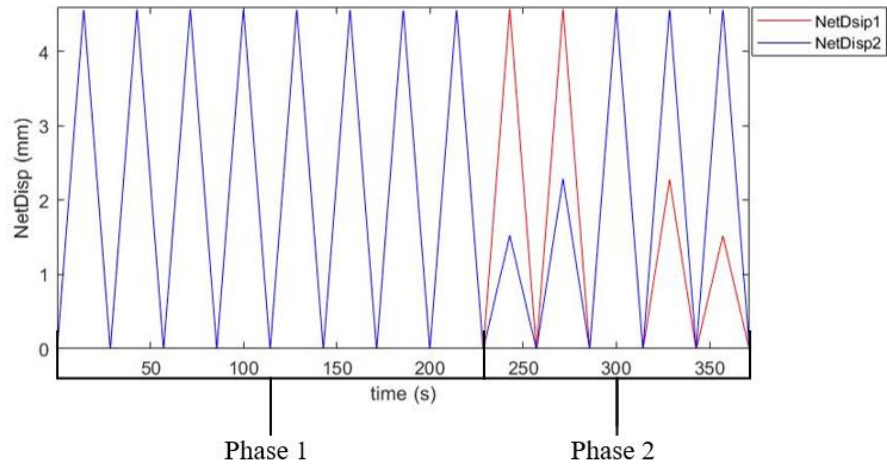


Figure 2.21 - Aorta displacement-controlled protocol example (raw data)

Table 2.6 and Table 2.7 show the amplitudes imposed to motors 1 and 2. Since motors 3 and 4 reproduced symmetrically their displacement ($\text{DispDiff}=0$), the actual amplitude applied on the specimens was doubled (see Figure 2.20 and Figure 2.21).

Load and displacement values were exported and matched with optical strain measurement mentioned above.

2.3.6. Markers segmentation

As previously pointed out, optical strain measurement is compulsory in soft biological tissue characterization. On this purpose, an image segmentation MATLAB routine has been developed. A single frame from the video relating to a GLU-treated aorta specimen will be used to describe the routine in the following paragraphs.

RGB image

Each frame of the recorded video was saved as an image in order to perform the segmentation.

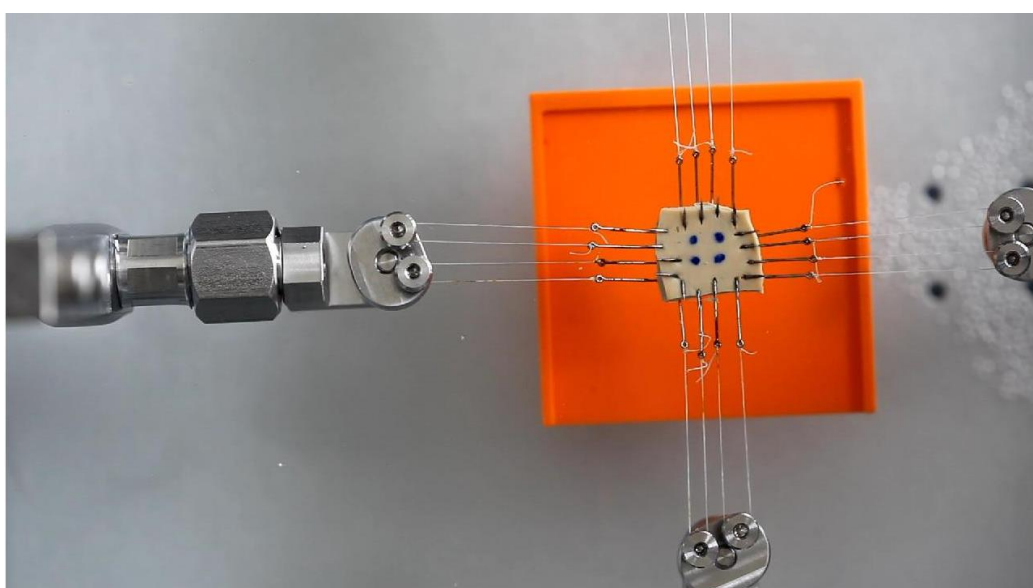


Figure 2.22 - RGB image

Greyscale image

Since the markers are blue, only the red layer of the image was utilized for the following steps in order to obtain the maximum contrast available. Indeed, the specimen is light-colored, so it would have been very bright in every RGB layer. Using the red or green layer allows to obtain black markers in the greyscale image. Red has been chosen because the support visible in the background is orange, so it was bright as well, enhancing the contrast with the markers.

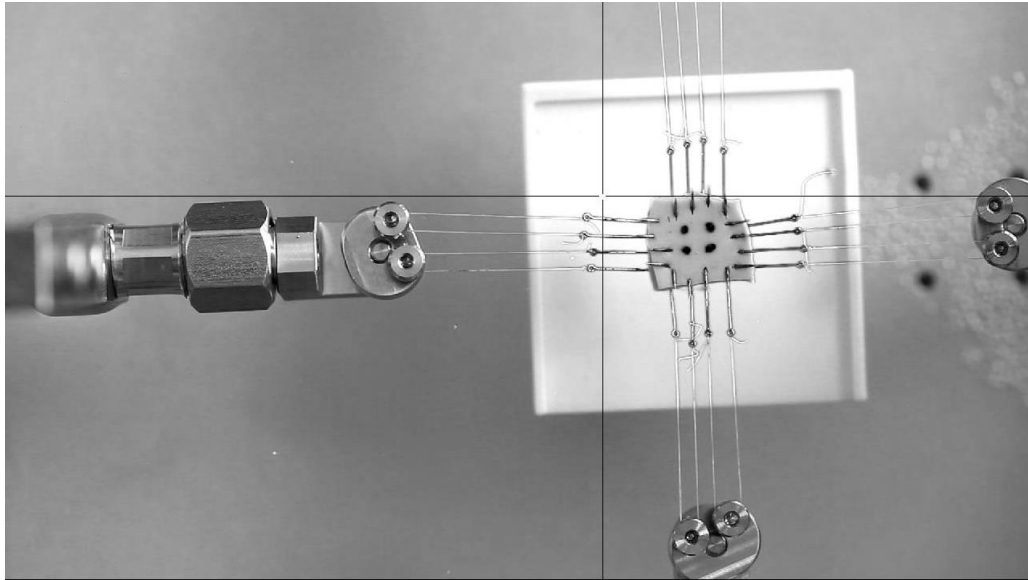


Figure 2.23 - Greyscale image

Image rotation

Next, the image was rotated in order to align the system axes to the image axes. The upper edge of the support was detected with an automatic routine using the selecting tool displayed in Figure 2.23, and its tilt angle was used to rotate the image. The length of the edge in pixels was measured as well, in order to calculate a conversion factor from pixel to mm for the entire image.

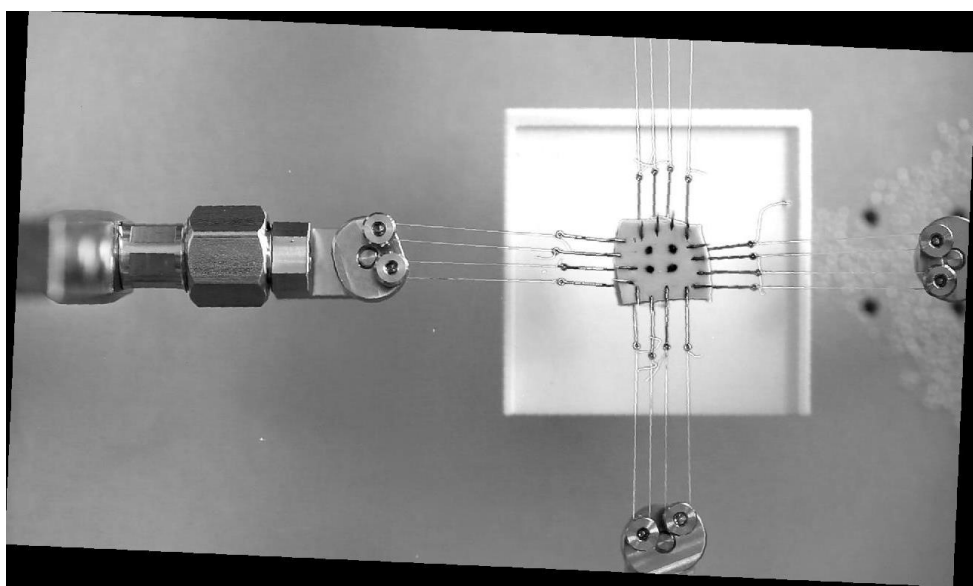


Figure 2.24 - Rotated image

Image clipping

The image was clipped in order to maintain just the region of interest for the strain computation. A large clip was performed to prevent markers from going out the shot in any frame.

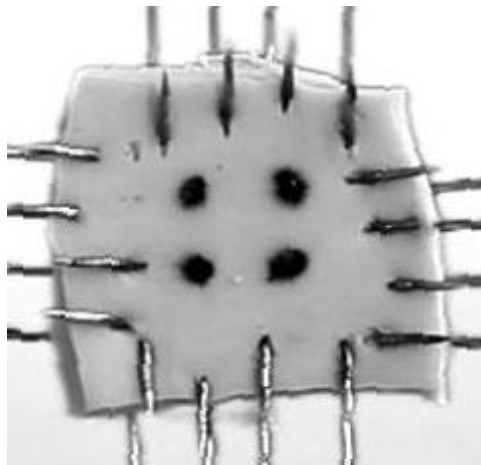


Figure 2.25 - Clipped image

Contrast enhancing

To simplify the following steps, a contrast enhancing routine was applied on the image.

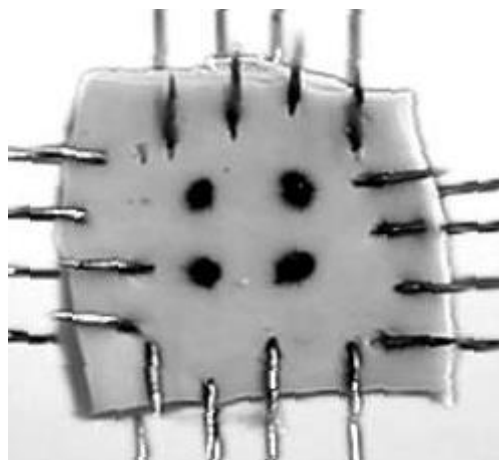


Figure 2.26 - Image with enhanced contrast

Binarization

A threshold was applied to binarize the image and obtain black markers on a white background.

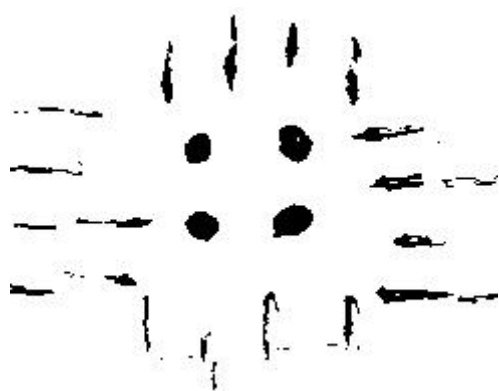


Figure 2.27 - Binary image

Complement

Since with the ROIs (regions of interest) on a black background were needed for the following steps, the complement of the image was obtained.

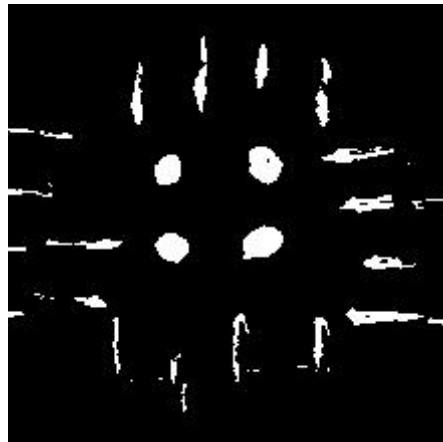


Figure 2.28 - Image complement

Noise suppression

A noise suppressor was applied to remove the littlest element of the image, which could have been recognized as circles by the routine in the following steps.

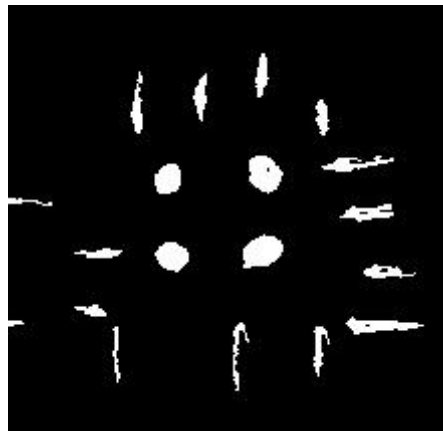


Figure 2.29 - Image after noise suppression

Circles detection

Circular regions were detected and smoothed with an automatic MATLAB routine.

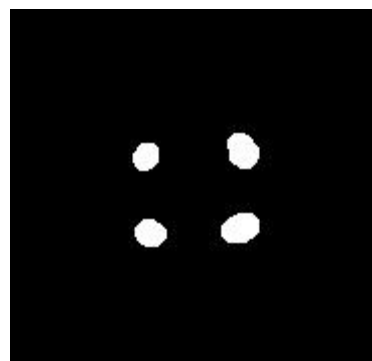


Figure 2.30 - Circular ROIs

Markers coordinates calculation

Finally, the four circular regions closest to the center of the image (the only ROIs in this example image) were recognized as markers and numerated in order to calculate their distances variation (i.e. the deformation of the central region of the specimen).



Figure 2.31 - Final image

The centroids of the so identified markers were used for strain computation as explained in paragraph 2.3.4.

2.3.7. Mechanical indexes and statistical analysis

The so computed strains, together with the load data exported from WinTest, were used to obtain stress-strain curves for the five cycles in the second phase of the displacement-controlled protocol. Since the curves could be divided in two nearly linear regions, the derivate of each stress-strain function was calculated and the abrupt change in its mean was detected with a MATLAB routine and used to split the curve in two regions. Each curve was then fitted with two segments and two different slopes were calculated. The figures below show two examples of the fitting.

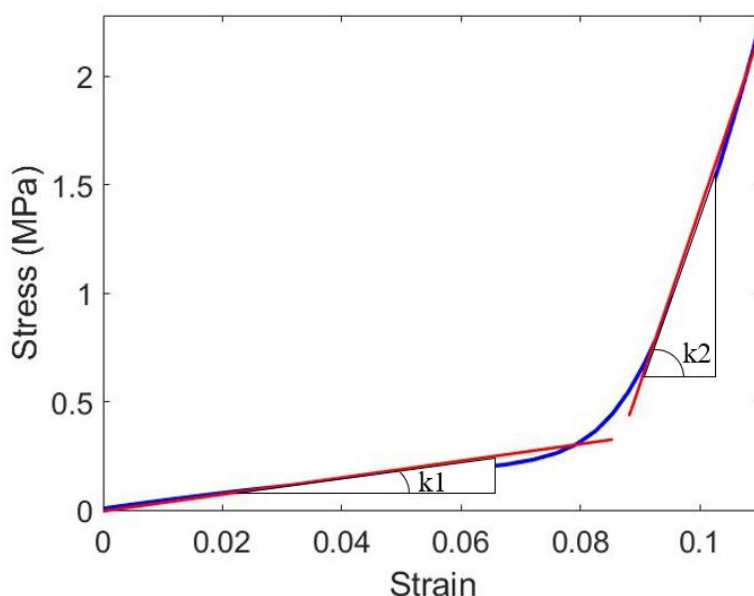


Figure 2.32 - Pericardium linear fitting example

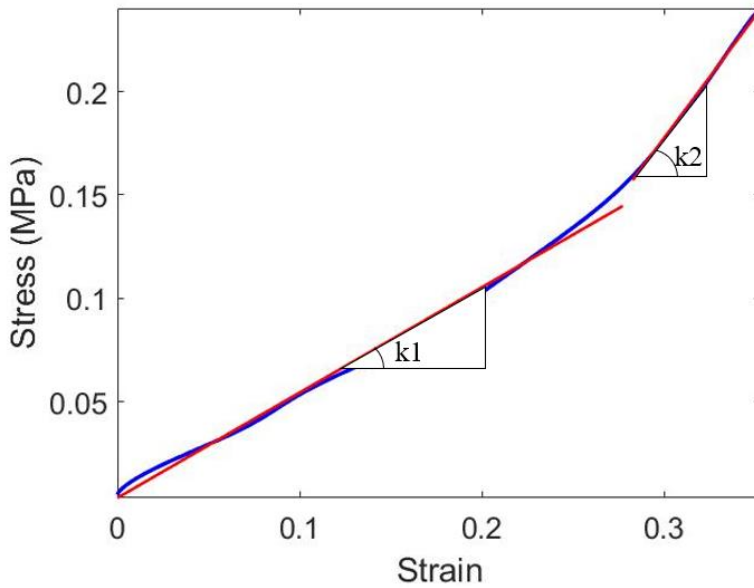


Figure 2.33 - Aorta linear fitting example

Thus, the slopes of each curve were calculated to estimate the stiffness of each sample, along each axis:

$$k = \frac{\delta(\text{stress})}{\delta(\text{strain})} [\text{MPa}]$$

The mean and standard deviation of the stiffness of each type of specimen (GAF and GLU-treated pericardium and aorta) were calculated to compare the two treatments. The k values obtained from the stress-strain curves related to specimens of the same type were averaged cycle per cycle and represented in the bar diagrams in the following chapter.

The curves were also compared with stress-strain curves obtained in previous works. Curves obtained from uniaxial tensile tests on fresh bovine pericardium along the collagen preferred and cross-preferred directions⁵⁵ were compared to pericardium specimens along the apex-base and circumferential directions respectively. Similarly, fresh porcine aorta stress-strain curves⁵⁶ were compared with aorta specimens tested in this work.

Finally, a three-way ANOVA was performed. This test represents a statistical technique which analyzes whether the average value of a variable is significantly influenced by different types of classifications of the data. In this case, the aim is to discover whether the treatments and the directions determine a significative difference in the stiffness of the specimens. The slopes were divided by curve region and tissue, obtaining four datasets:

- aorta, first region (k1);
- aorta, second region (k2);
- pericardium, first region (k1);
- pericardium, second region (k2).

Treatments (GLU and GAF), directions (axis 1 or 2) and cycles of the second phase of the protocol (1 to 5) were taken in consideration as variability factors, while the slope was the dependent variable; 0.05 was taken as a significance threshold for the p-value.

3. Results and discussion

3.1. Stress-strain curves

The data obtained and elaborated as described above, will be detailed in this chapter. The following figures show the stress-strain curves of each sample during the second phase of the displacement-controlled protocol. The curves were divided in four different charts, each chart represents the data of the same tissue specimens along the same axis. Solid lines were used to draw the curves of GAF-treated tissues and dashed lines were adopted for the GLU-treated ones.

Cycle 3 in each figure corresponds to the maximum wave amplitude applied along both directions. Indeed, the highest stresses can be observed in this cycle for every specimen along both axes. Stresses in the other curves are lower because in cycles 1 and 2, only $\frac{1}{3}$ and $\frac{1}{2}$ of the maximum displacement were applied along axis 2. Similarly, the same results occur in cycles 4 and 5 because a lower displacement is applied along axis 1.

Axis 1 is aligned with the circumferential direction of aorta and pericardium specimens. Axis 2 is along the longitudinal and apex-base directions respectively. However, the estimation of physiological direction for the most part of aorta specimens was quite difficult and inaccurate. Indeed, the specimens were provided in an already cut form and the directions were hypothesized, when possible, according to the curvature of the specimens.

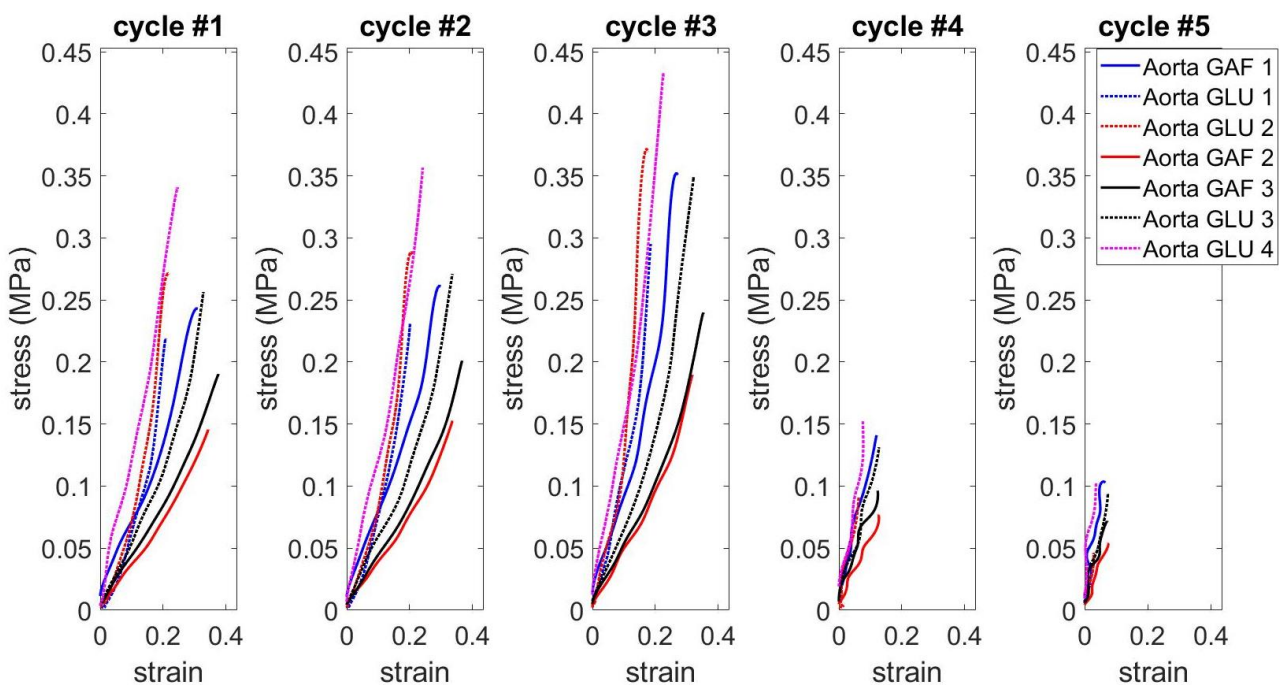


Figure 3.1 - Aorta stress vs strain axis 1

Figure 3.1 refers to the circumferential direction of aorta specimens. Specimens ‘Aorta GAF 2’ and ‘Aorta GAF 3’ have lower values of stress and highest strains compared to the GLU-treated

specimens. However, ‘Aorta GAF 1’, which curve is drawn with a solid blue line, has similar values compared with these last. For this reason, no substantial differences between the two treatments can be observed in these graphs.

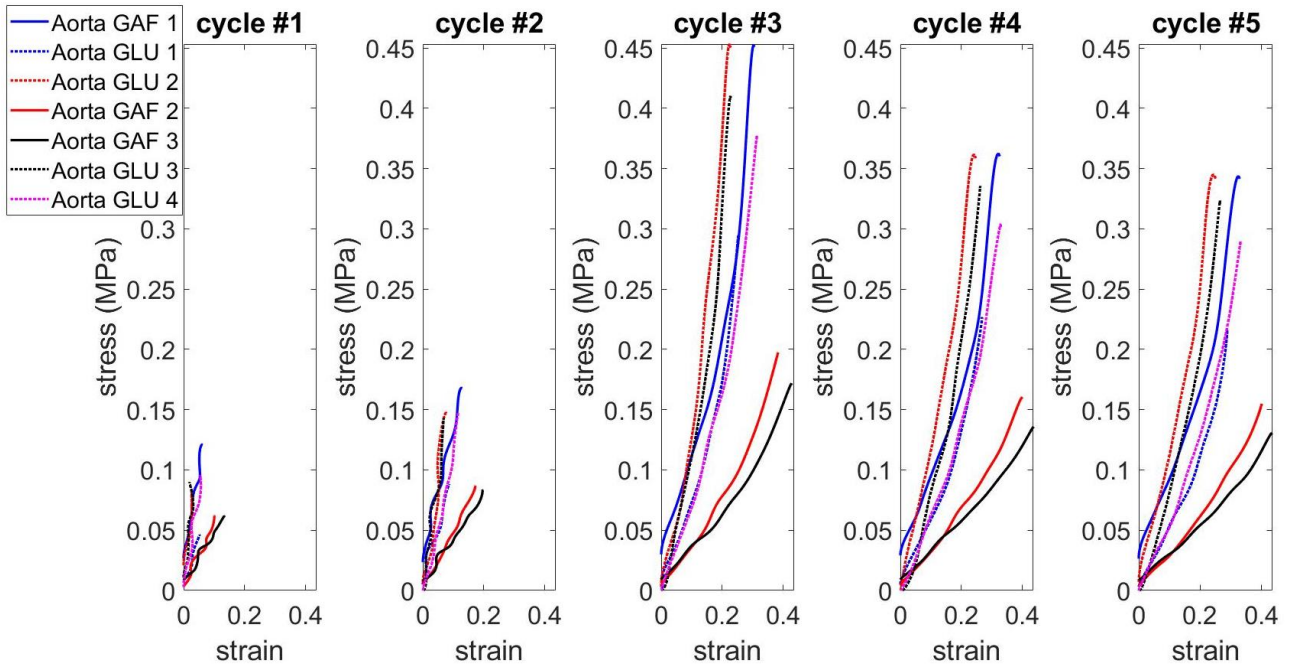


Figure 3.2 - Aorta stress vs strain axis 2

Figure 3.2 shows the longitudinal direction for aorta specimens. Again, a different behavior can be observed in the 2nd and 3rd GAF-treated aortas in respect to the others. With the limited number of specimens available is hard to state if this difference is related to the treatment.

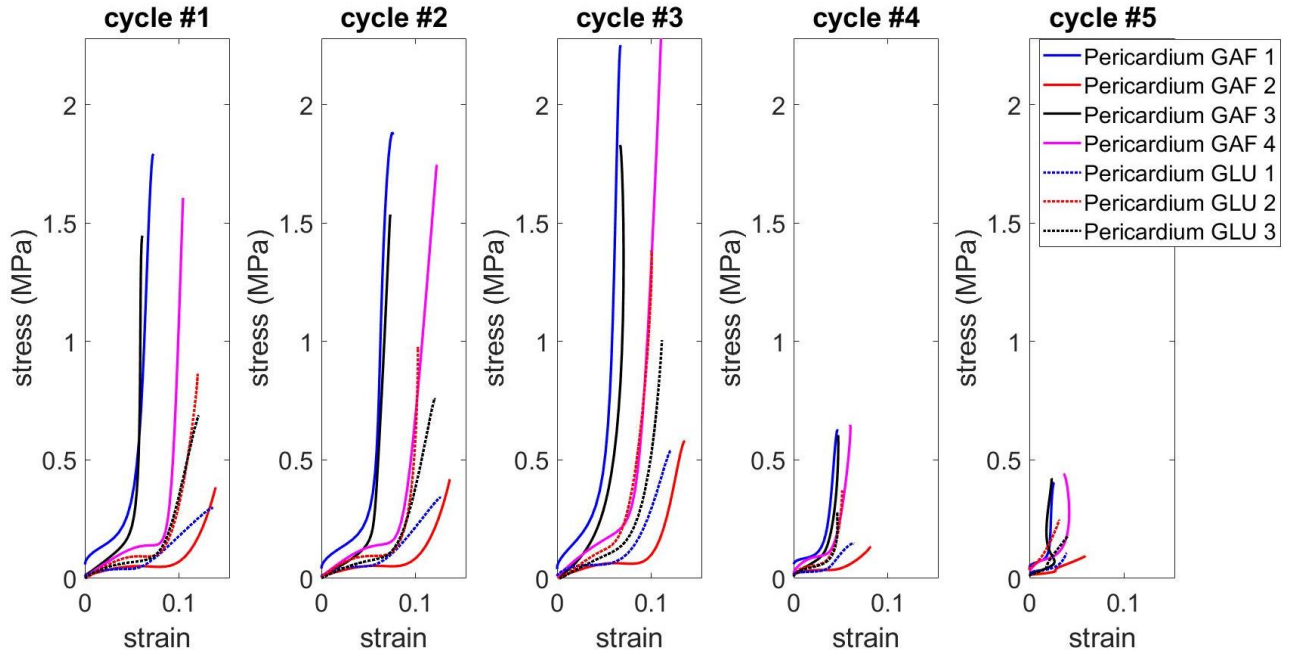


Figure 3.3 - Pericardium stress vs strain axis 1

The curves for the circumferential direction of pericardium specimens is shown in Figure 3.3. In contrast to what can be seen in the previous graphs, GAF-treated tissues are apparently stiffer than

GLU-treated ones. The solid red line, however, represents a GAF-treated pericardium, which seems to be the most pliant.

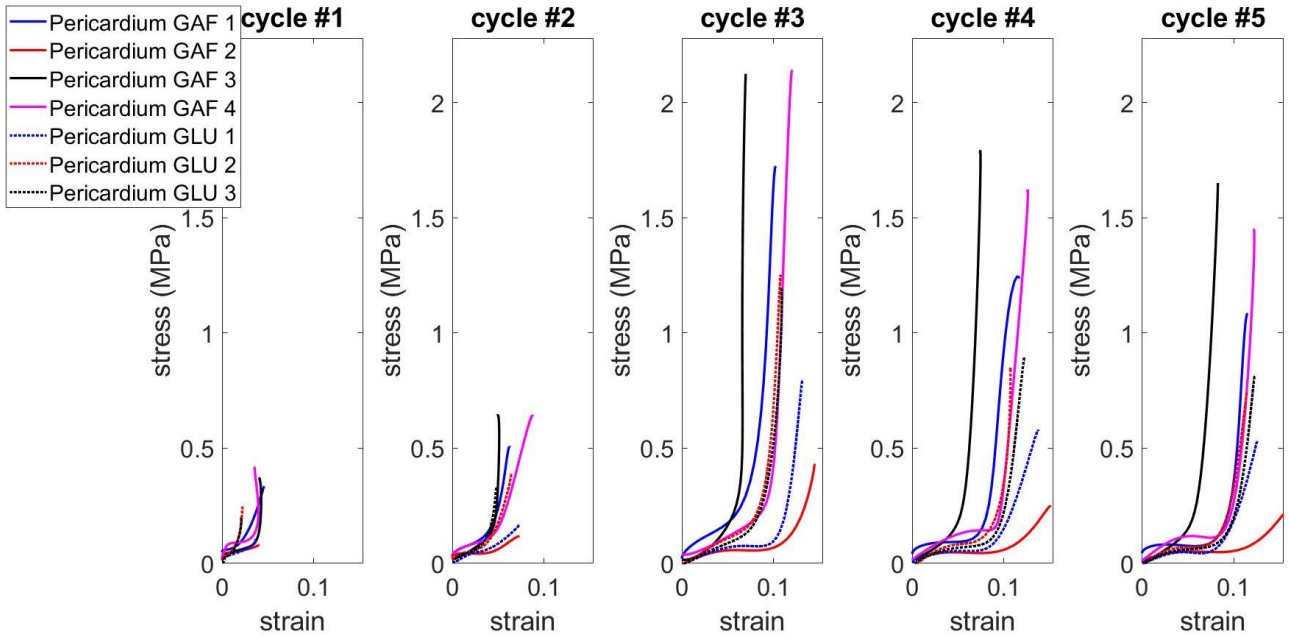


Figure 3.4 - Pericardium stress vs strain axis 2

The results observed in Figure 3.3 are confirmed in Figure 3.4, which shows the data along the apex-base direction of pericardium tissues. The trends are strongly specimen-specific, and no reliable considerations can be done by the only observation of the curves.

3.1.1. Literature comparison

The curves of 3rd cycle of each figure shown so far in this chapter, were compared to stress-strain curves obtained in previous works. In the following figures, the curves relative to GAF-treated tissues are drawn in blue, while the GLU curves are red. Both aorta and pericardium were compared to fresh tissue along both axes; the relative curves are green in the charts.

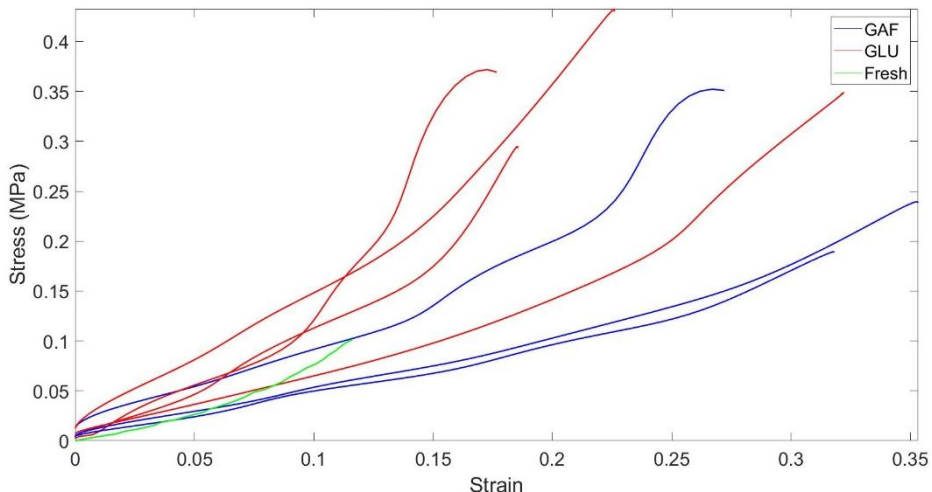


Figure 3.5 - Aorta axis 1 literature comparison

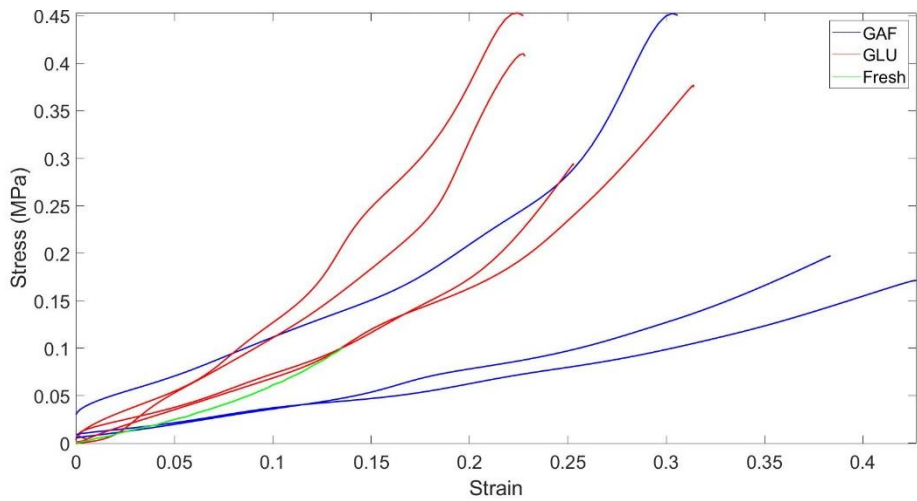


Figure 3.6 - Aorta axis 2 literature comparison

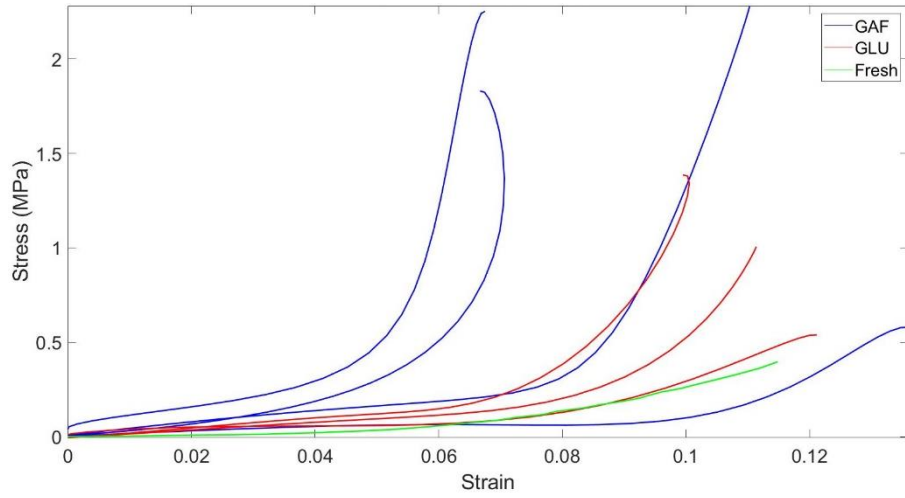


Figure 3.7 - Pericardium axis 1 literature comparison

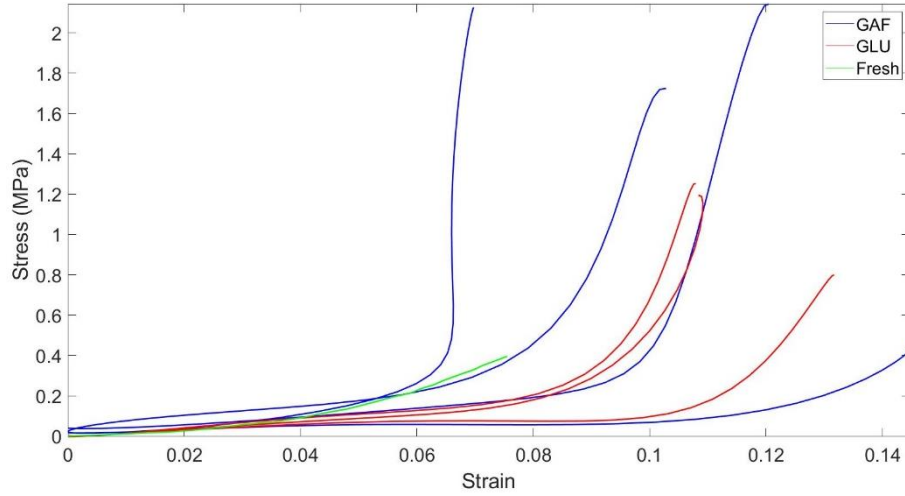


Figure 3.8 - Pericardium axis 2 literature comparison

In the tests taken in consideration, both aorta⁵⁶ and pericardium⁵⁵ underwent lower values of strain and stress compared with those applied in this work, while the curves trend looks similar in all cases.

All green curves are positioned between the other curves and this makes difficult to state which treatment produces a more fresh-like tissue.

3.2. Stiffness estimation and statistical analysis

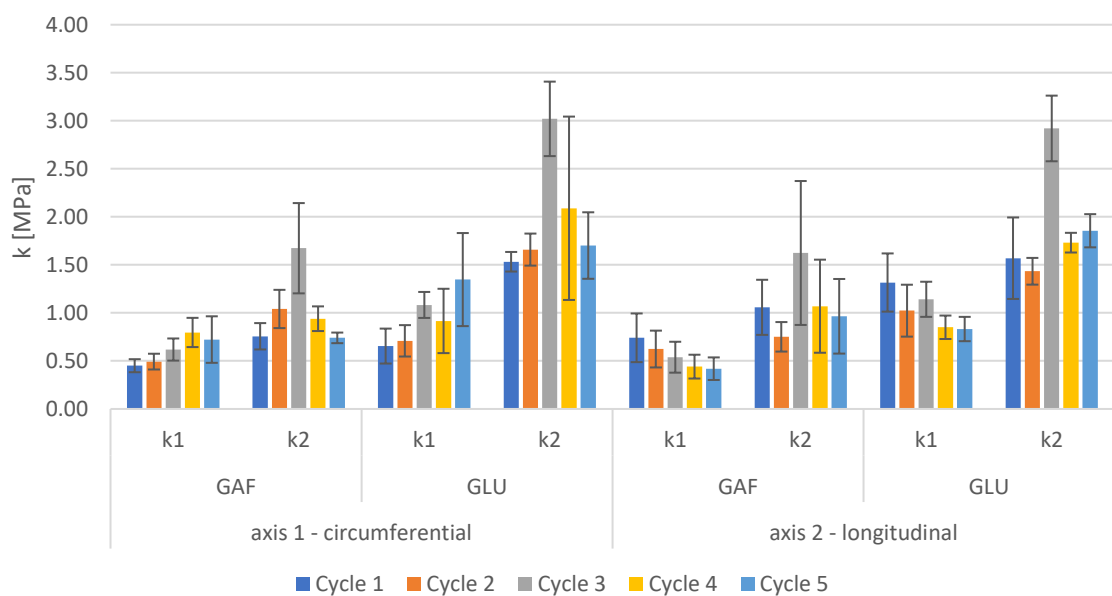
3.2.1. The Aorta

Two slopes

Initially, both slope values, which are referred to as k_1 and k_2 in the following diagrams and tables, were taken in consideration for all specimens. The charts represent the slope of the curves averaged among the same-tissue, same-treatment specimens. Each bar, indeed, represents the mean slope of a certain cycle, along a certain axis for all the specimens of the same type, and its standard deviation. For representation reasons, in the bar diagrams each slope is represented as mean \pm std/2, the total values of standard deviation are shown in the tables.

Table 3.1 - Aorta stiffness estimation

Axis 1 - circumferential				Axis 2 - longitudinal			
GAF		GLU		GAF		GLU	
k_1	k_2	k_1	k_2	k_1	k_2	k_1	k_2
0.45 \pm 0.14	0.76 \pm 0.27	0.65 \pm 0.36	1.53 \pm 0.20	0.74 \pm 0.51	1.06 \pm 0.57	1.32 \pm 0.61	1.57 \pm 0.85
0.49 \pm 0.16	1.04 \pm 0.40	0.71 \pm 0.33	1.66 \pm 0.33	0.62 \pm 0.38	0.75 \pm 0.31	1.02 \pm 0.54	1.43 \pm 0.28
0.62 \pm 0.23	1.67 \pm 0.94	1.08 \pm 0.27	3.02 \pm 0.78	0.54 \pm 0.32	1.62 \pm 1.50	1.14 \pm 0.37	2.92 \pm 0.68
0.80 \pm 0.30	0.94 \pm 0.26	0.92 \pm 0.67	2.09 \pm 1.91	0.44 \pm 0.25	1.07 \pm 0.97	0.85 \pm 0.24	1.73 \pm 0.20
0.72 \pm 0.48	0.74 \pm 0.11	1.35 \pm 0.97	1.70 \pm 0.69	0.42 \pm 0.23	0.96 \pm 0.78	0.83 \pm 0.25	1.86 \pm 0.35



Graph 3.1 - Aorta stiffness estimation

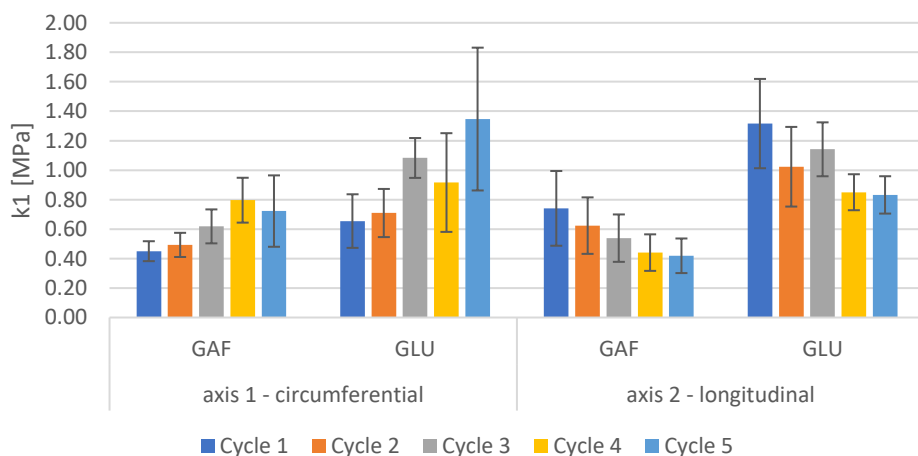
As can be also seen in Figure 3.1 and Figure 3.2, k_2 is higher than k_1 for each type of sample and in both directions. The GLU-treated tissues are stiffer than GAF-treated ones. No differences can be observed between the two directions in this diagram.

One slope: k_1

The following table and chart only represent the slope of the first region of each curve, namely k_1 .

Table 3.2 - Aorta first region stiffness estimation

Axis 1 - circumferential		Axis 2 - longitudinal	
GAF	GLU	GAF	GLU
k_1	k_1	k_1	k_1
0.45 ± 0.14	0.65 ± 0.36	0.74 ± 0.51	1.32 ± 0.61
0.49 ± 0.16	0.71 ± 0.33	0.62 ± 0.38	1.02 ± 0.54
0.62 ± 0.23	1.08 ± 0.27	0.54 ± 0.32	1.14 ± 0.37
0.80 ± 0.30	0.92 ± 0.67	0.44 ± 0.25	0.85 ± 0.24
0.72 ± 0.48	1.35 ± 0.97	0.42 ± 0.23	0.83 ± 0.25



Graph 3.2 - Aorta first region stiffness estimation

Graph 3.2 shows that the GLU-treatment apparently produces a stiffer tissue along both axes. No recurring differences can be observed between the two axes neither between the different cycles of the protocol.

Statistical analysis

Table 3.3 shows the p-value resulting from the three-way ANOVA described in paragraph 2.3.7.

Table 3.3 - Aorta k_1 p-values

Treatments	Axes	Cycles
3.46E-04	0.82	0.88

Since the significative discriminant is 0.5, the treatments affect the mechanical properties, according to the ANOVA results, while the axes and the cycles do not.

The results relative to the treatments are shown in Figure 3.9, which shows the significant difference in the stiffness obtained with different treatments.

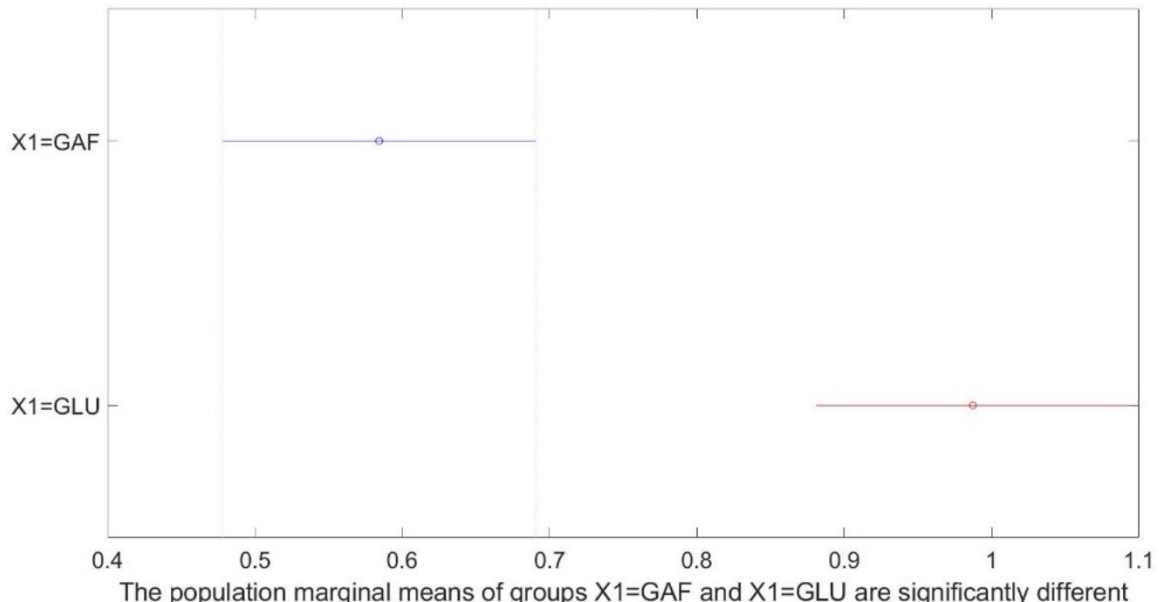


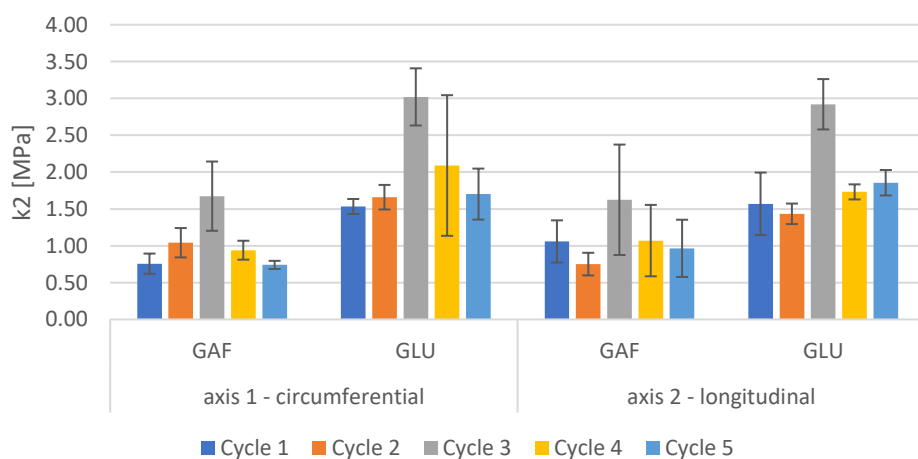
Figure 3.9 - Aorta $k1$ treatment difference

One slope: $k2$

The analysis about slope in second region of aorta curves is described in this paragraph.

Table 3.4 - Aorta second region stiffness estimation

Axis 1 - circumferential		Axis 2 - longitudinal	
GAF	GLU	GAF	GLU
$k2$	$k2$	$k2$	$k2$
0.76 ± 0.27	1.53 ± 0.20	1.06 ± 0.57	1.57 ± 0.85
1.04 ± 0.40	1.66 ± 0.33	0.75 ± 0.31	1.43 ± 0.28
1.67 ± 0.94	3.02 ± 0.78	1.62 ± 1.50	2.92 ± 0.68
0.94 ± 0.26	2.09 ± 1.91	1.07 ± 0.97	1.73 ± 0.20
0.74 ± 0.11	1.70 ± 0.69	0.96 ± 0.78	1.86 ± 0.35



Graph 3.3 - Aorta second region stiffness estimation

As seen for the first region of the curve, the slope of the curves is higher for GLU-treated tissues than GAF-treated one. In this case, the maximum slope is recorded during the 3rd cycle, when both directions undergo the maximum displacement.

Statistical analysis

Table 3.5 - Aorta k2 p-values

Treatments	Axes	Cycles
2.27E-06	0.86	2.27E-04

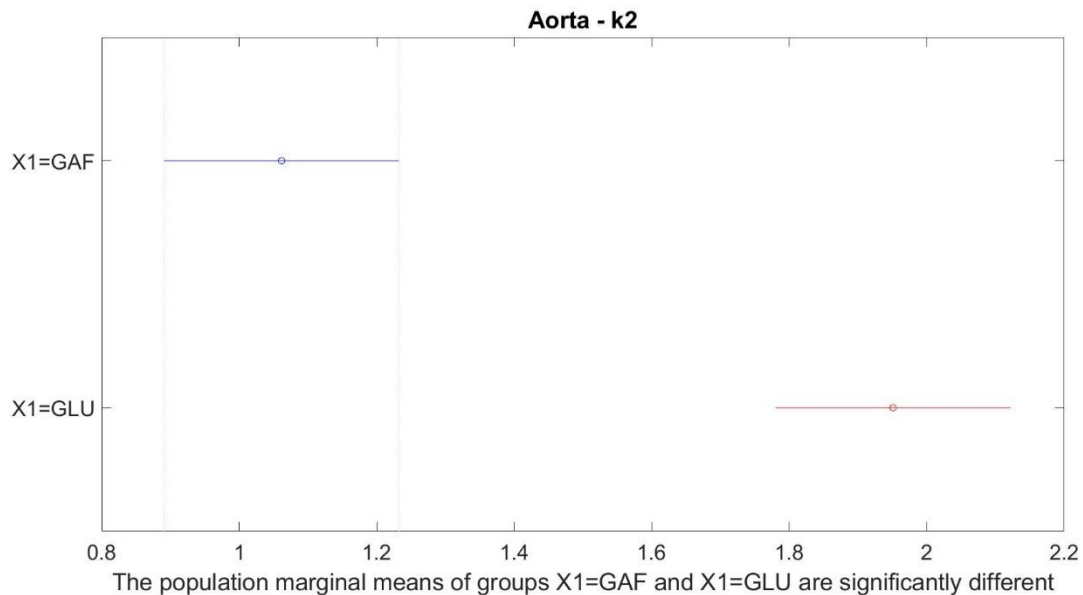


Figure 3.10 - Aorta k2 treatment difference

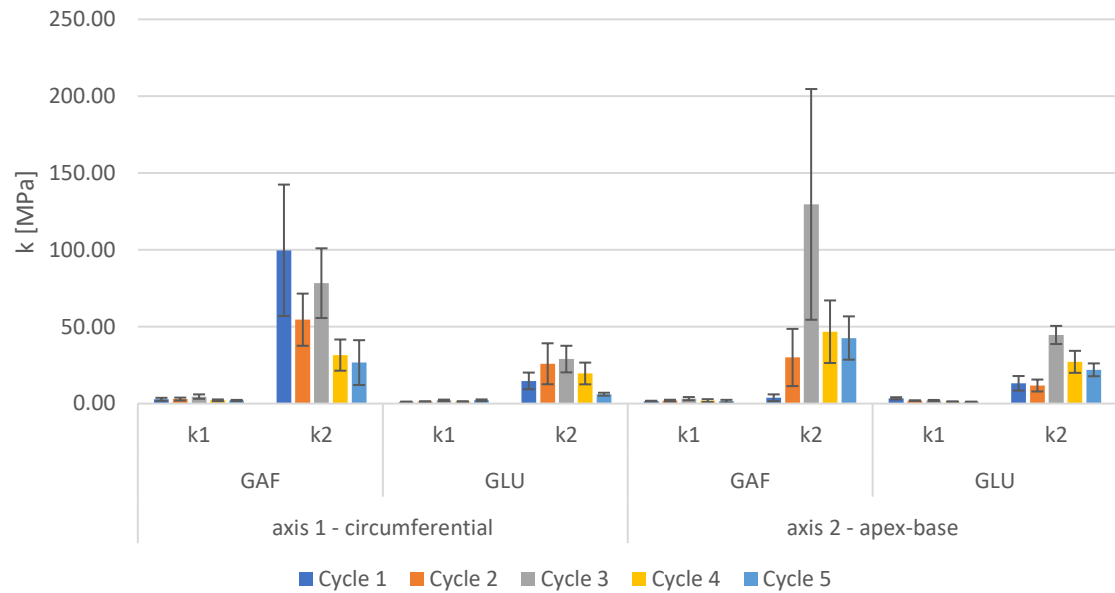
In this case, the cycles influenced the stiffness of the specimens as well as the treatment, as can be noticed from the p-value, which is lower than the established threshold $p=0.05$.

3.2.2. The pericardium

Two slopes

Table 3.6 - Pericardium stiffness estimation

Axis 1 - circumferential				Axis 2 - longitudinal			
GAF		GLU		GAF		GLU	
k1	k2	k1	k2	k1	k2	k1	k2
2.81 ± 1.90	99.70 ± 85.59	1.09 ± 0.42	14.75 ± 10.85	1.60 ± 0.47	3.80 ± 4.37	3.42 ± 1.42	13.19 ± 9.47
2.95 ± 1.87	54.58 ± 33.93	1.28 ± 0.35	25.89 ± 26.66	1.89 ± 1.23	29.99 ± 37.26	1.89 ± 0.52	11.75 ± 7.77
4.54 ± 2.88	78.35 ± 45.36	2.07 ± 1.04	28.95 ± 17.34	3.19 ± 2.08	129.59 ± 150.12	1.94 ± 0.83	44.65 ± 11.80
2.09 ± 1.23	31.53 ± 20.31	1.24 ± 0.61	19.59 ± 14.14	1.95 ± 1.85	46.76 ± 40.69	1.21 ± 0.48	27.16 ± 14.31
1.98 ± 0.83	26.67 ± 29.16	2.14 ± 1.14	6.10 ± 1.91	1.58 ± 1.71	42.65 ± 28.17	1.11 ± 0.34	21.96 ± 8.37



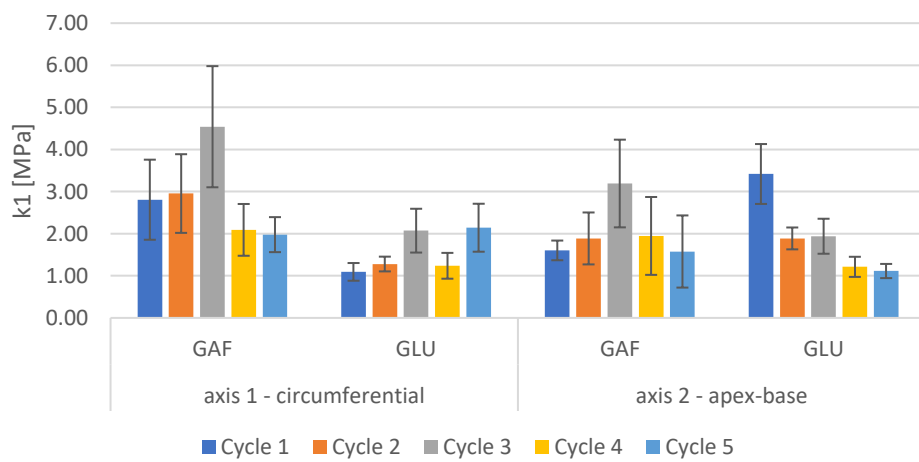
Graph 3.4 - Pericardium stiffness estimation

The pericardium shows a very different behavior in the two parts of the stress-strain curves. The values of k_2 are significantly higher than k_1 ones. Indeed, the stress-strain curve tend to rear up, becoming nearly vertical. Since k_1 is non observable using the same scale as k_2 , in the following paragraphs the two regions of the curves will be discussed separately.

One slope: k_1

Table 3.7 - Pericardium first region stiffness estimation

Axis 1 - circumferential		Axis 2 - longitudinal	
GAF	GLU	GAF	GLU
k_1	k_1	k_1	k_1
2.81 ± 1.90	1.09 ± 0.42	1.60 ± 0.47	3.42 ± 1.42
2.95 ± 1.87	1.28 ± 0.35	1.89 ± 1.23	1.89 ± 0.52
4.54 ± 2.88	2.07 ± 1.04	3.19 ± 2.08	1.94 ± 0.83
2.09 ± 1.23	1.24 ± 0.61	1.95 ± 1.85	1.21 ± 0.48
1.98 ± 0.83	2.14 ± 1.14	1.58 ± 1.71	1.11 ± 0.34



Graph 3.5 - Pericardium first region stiffness estimation

In the case of pericardium, the results are less repetitive than the previous ones. The greatest slope is registered in the central cycle, while both axes are stretched with the maximum amplitude, for the GAF-treated specimens. GLU-treated specimens have a greater slope in correspondence of the 5th cycle along axis 1 and of the 1st cycle along axis 2.

Statistical analysis

Table 3.8 - Pericardium k1 p-values

Treatments	Axes	Cycles
0.04	0.34	0.08

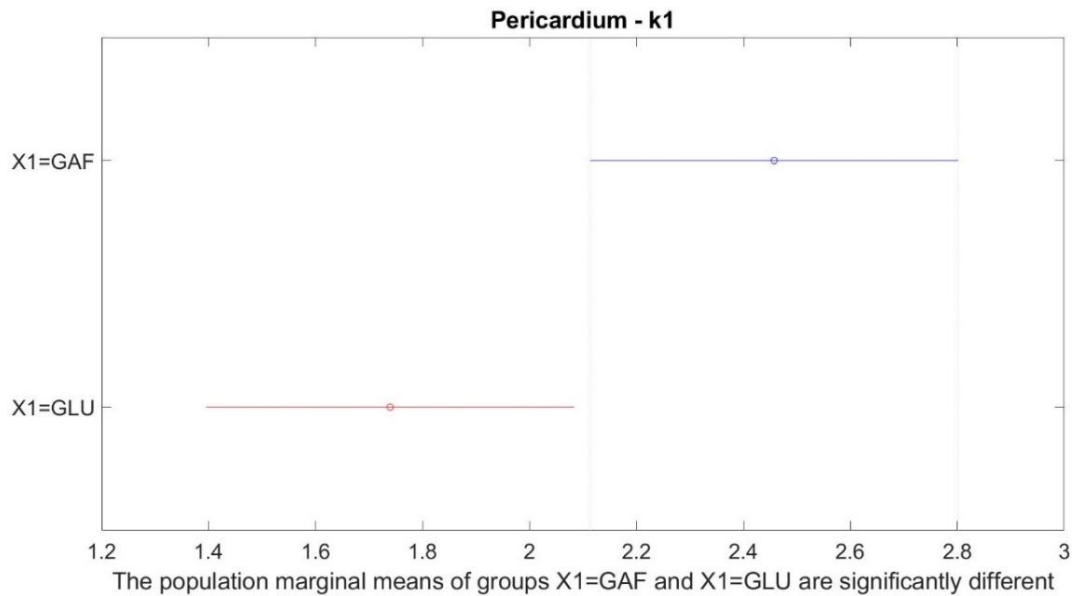


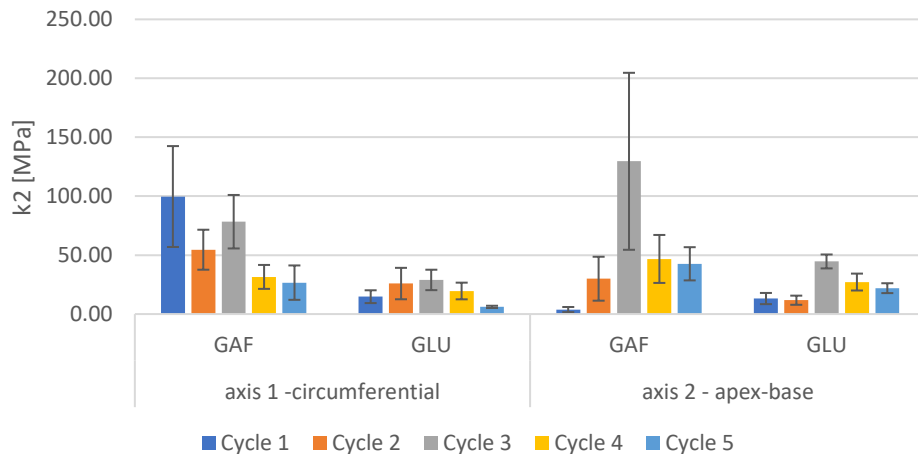
Figure 3.11 - Pericardium k1 treatment difference

Pericardium stiffness in the first region of the curves is influenced by treatments, as seen before. Cycles and axes do not affect the slope.

One slope: k2

Table 3.9 - Pericardium second region stiffness estimation

Axis 1 - circumferential		Axis 2 - longitudinal	
GAF	GLU	GAF	GLU
k2	k2	k2	k2
99.70 ± 85.59	14.75 ± 10.85	3.80 ± 4.37	13.19 ± 9.47
54.58 ± 33.93	25.89 ± 26.66	29.99 ± 37.26	11.75 ± 7.77
78.35 ± 45.36	28.95 ± 17.34	129.59 ± 150.12	44.65 ± 11.80
31.53 ± 20.31	19.59 ± 14.14	46.76 ± 40.69	27.16 ± 14.31
26.67 ± 29.16	6.10 ± 1.91	42.65 ± 28.17	21.96 ± 8.37



Graph 3.6 - Pericardium second region stiffness estimation

As seen before, the highest value of slope corresponds to the 3rd cycle in the most part of the specimens. The differences between the two treatments are more visible in this case: the GAF produces a significantly stiffer tissue along both axes.

Statistical analysis

Table 3.10 - Pericardium k2 p-values

Treatments	Axes	Cycles
0.01	0.84	0.07

Treatments produce significantly different result in stiffness also in this last dataset. Again, the p-values related to axes and cycles are greater than the threshold.

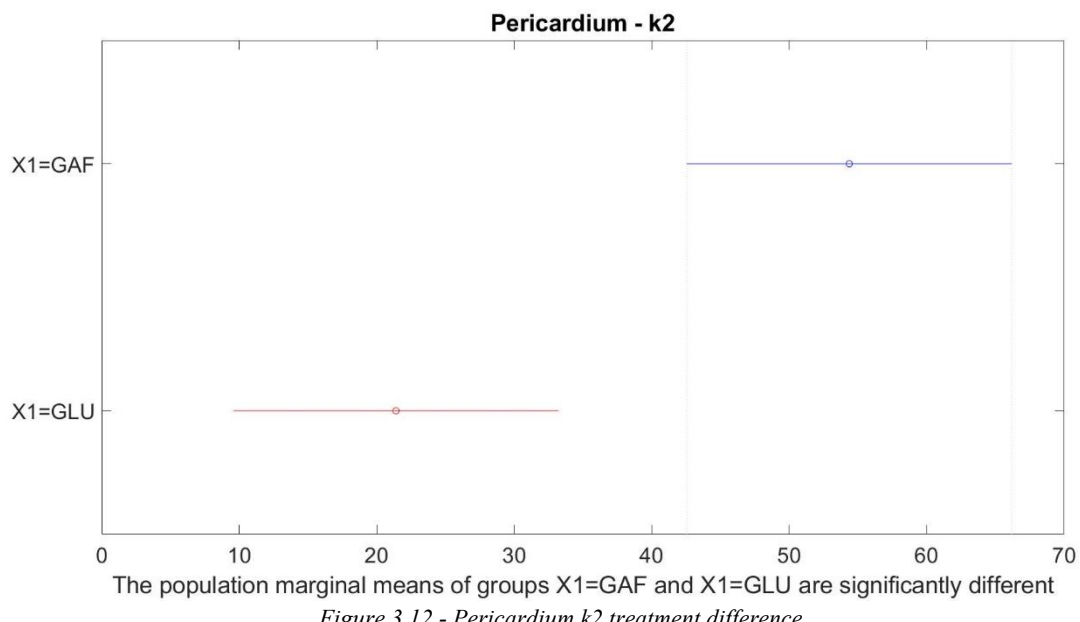


Figure 3.12 - Pericardium k2 treatment difference

4. Conclusions

In this work, a testing protocol for mechanical biaxial characterization of soft tissues was devised. It was applied on porcine aorta and bovine pericardium, decellularized with two different chemical agents: glutaraldehyde and acid-free glyoxal. The process consisted in several phases. First, the samples were cut in square shaped specimens, which underwent thickness measurement. The use of CNC controlled scanning probe allowed to perform a rapid calculation of the thickness, since each scan lasted about one minute. This is a crucial aspect of the measurement because the specimens should rest out of their storing solution for as little time as possible in order to avoid dehydration, which would permanently change the mechanical properties of the tissue. Thickness measurement is the only phase of the process during which the specimens are not immersed in an aqueous medium, so it must be very fast.

After thickness measurement, the specimens underwent the mechanical tests. Each test started with the preparation of the specimen, i.e. the insertion of the hooks and the drawing of the markers in the central region. This phase was awkward because the soft tissues are difficult to handle. However, the fixture provided by TA instruments facilitated the work and allowed a repeatable and quite precise positioning of the specimens in the gripping system. A valid drawing of the markers was also achieved after trying different methods. First, graphite markers were glued on the surface of the specimens with cyanoacrylate glue, but it used to become stiffer in water and would have compromised the mechanical properties of the tissue. Water resistant permanent ink was the final choice; a ‘trial and error’ process was performed to select the optimal color to obtain the maximum contrast available in each frame of the videos recorded during the tests.

Then, the first set of specimens was tested with a load-controlled protocol. It proved to be not repeatable and hard to control. Moreover, the lack of control resulted in the destruction of few specimens. For these reasons, a displacement-controlled test was devised and utilized for the characterization of the most part of the specimens. The last version of the biaxial mechanical test is faster, more repeatable and easier to perform compared to the first one. Indeed, displacement-controlled tests performed with ElectroForce LM1 TestBench Test Instrument do not require a tuning process. Since it was a critical aspect of this work and made the load-controlled protocol specimen-specific, its absence resulted in a quicker test which was more generalized and avoided rupture and unexpected behaviors of the specimens.

Finally, the data processing was performed with MATLAB custom routines, as well as the optical strain computation. The color and shape of the markers was very important in order to perform a correct segmentation of the images. The contrast between the markers and the background, together with the precision in the circular form of the markers themselves, made the difference between a

noisy segmentation and a good one. Stress-strain curves were obtained and used to estimate the stiffness of the samples. The aim was to establish whether the two different types of treatment produced tissues with different stiffness.

A three-way ANOVA allowed to determine that the treatments affect the stiffness of the tissues. Indeed, the pericardium is characterized by a greater slope when treated with acid-free glyoxal. Aorta, in turn, is stiffer when it undergoes a glutaraldehyde treatment. The specimens shown a different stiffness cycle by cycle in some cases, but the population marginal means obtained in the statistical analysis were not significantly different. The stiffness was expected to change also between one axis and another, since it should be linked with collagen fibers directions. However, it did not happen. This result is likely correlated to the fact that anatomical directions were taken in consideration during the tests. In details, the pericardium specimens were cut with edges parallel to the apex-base and circumferential directions. Similarly, longitudinal and circumferential directions were considered for aorta. However, what affects the mechanical properties is the preferred direction of collagen fibers, which was not determined before the tests and is not always correspondent with anatomical directions. This represents the major limit of this work. Before future tests, the collagen directions should be determined optically or mechanically. Mechanical tests could be destructive or change the mechanical properties of the tissue, thus are not advisable for a preliminary estimation of the directions. Small angle light scattering (SALS) could be a valid instrument. It is an optical method which has been used before to map the collagen fibers directions in pericardial sac.⁵⁷

Other future works might be a coupled protocol of biaxial and uniaxial test or a study of the microscale mechanical properties of the tissue (i.e. nanoindentation) before macroscopic biaxial test. Moreover, a constitutive model could be fitted on further results.

Bibliography

1. Holt, J. P. The normal pericardium. *Am. J. Cardiol.* **26**, 455–465 (1970).
2. Netter, F. H. *Atlas of human anatomy*.
3. OpenStax College. *Anatomy & Physiology*. OpenStax College (2013).
4. Ishihara, T. *et al.* Histologic and ultrastructural features of normal human parietal pericardium. *Am. J. Cardiol.* **46**, 744–753 (1980).
5. Simionescu, D. T. & Kefalides, N. A. The biosynthesis of proteoglycans and interstitial collagens by bovine pericardial fibroblasts. *Exp. Cell Res.* **195**, 171–176 (1991).
6. Sibilla, S., Godfrey, M., Brewer, S., Budh-Raja, A. & Genovese, L. An overview of the beneficial effects of hydrolysed collagen as a nutraceutical on skin properties: Scientific background and clinical studies. *Open Nutraceuticals J.* **8**, 29–42 (2015).
7. Ricard-Blum, S. The Collagen Family. *Cold Spring Harb. Perspect. Biol.* **3**, 1–19 (2011).
8. Naimark, W. A., Lee, J. M., Limeback, H. & Cheung, D. T. Correlation of structure and viscoelastic properties in the pericardia of four mammalian species. *Am. J. Physiol. Circ. Physiol.* **263**, H1095–H1106 (1992).
9. Rémi, E. *et al.* Chapter 22 - Pericardial Processing: Challenges, Outcomes and Future Prospects. in *BIOMATERIALS SCIENCE AND ENGINEERING* Edited by Rosario Pignatello 3–30 (2011).
10. Hiester, E. D. & Sacks, M. S. Optimal bovine pericardial tissue selection sites . II . Cartographic analysis. (1997).
11. Martini, F. H., Timmons, M. J. & Tallitsch, R. B. *Human Anatomy*. (2012).
12. Gross, L. & Kugel, M. A. Topographic Anatomy and Histology of the Valves in the Human Heart. *Am. J. Pathol.* **7**, 445-474.7 (1931).
13. Porth, C. *Fisiopatología*. (1987).
14. Musumeci, L. *et al.* Prosthetic Aortic Valves: Challenges and Solutions. *Front. Cardiovasc. Med.* **5**, 1–5 (2018).
15. Head, S. J., Çelik, M. & Kappetein, A. P. Mechanical versus bioprosthetic aortic valve replacement. *Eur. Heart J.* **38**, 2183–2191 (2017).
16. Bloomfield, P. Choice of heart valve prosthesis. *Heart* **87**, 583–589 (2002).
17. Kerr, M., Wheatley, D. & Gourlay, T. The aortic valve: Structure, complications and implications for transcatheter aortic valve replacement. *Perfusion* (2014). doi:10.1177/0267659114521650
18. Vesely, I. Heart valve tissue engineering. *Circ. Res.* **97**, 743–755 (2005).

19. Khor, E. Methods for the treatment of collagenous tissues for bioprostheses. *Biomaterials* **18**, 95–105 (1997).
20. Garter, L. & Hiatt, J. *Color atlas and text of histology*. (2013).
21. Trentin, C., Faggiano, E., Conti, M. & Auricchio, F. *An automatic tool for thoracic aorta segmentation and 3D geometric analysis*. (2015). doi:10.1109/ISPA.2015.7306033
22. Almeida, V. New methods for hemodynamic evaluation : a multi-parametric approach. (2013).
23. Komutrattananont, P., Mahakkanukrauh, P. & Das, S. Morphology of the human aorta and age-related changes : anatomical facts. 109–114 (2019).
24. Augoustides, J. G. & Cheung, A. T. Chapter 19 - Aneurysms and Dissections. in *Perioperative Transesophageal Echocardiography: A companion to Kaplan's Cardiac Anesthesia* 191–217 (Elsevier Inc., 2013). doi:10.1016/B978-1-4557-0761-4.00019-0
25. Meuschke, M. *et al.* Visual Analysis of Aneurysm Data using Statistical Graphics. *IEEE Trans. Vis. Comput. Graph.* **25**, 997–1007 (2019).
26. Bentall, H. & De Bono, A. A technique for complete replacement of the ascending aorta. *Thorax* **23**, 338–339 (1968).
27. Negishi, J. *et al.* Evaluation of small-diameter vascular grafts reconstructed from decellularized aorta sheets. *J. Biomed. Mater. Res. - Part A* **105**, 1293–1298 (2017).
28. Wang, X. N., Chen, C. Z., Yang, M. & Gu, Y. J. Implantation of decellularized small-caliber vascular xenografts with and without surface heparin treatment. *Artif. Organs* **31**, 99–104 (2007).
29. Wu, P. *et al.* Decellularized porcine aortic intima-media as a potential cardiovascular biomaterial. *Interact. Cardiovasc. Thorac. Surg.* **21**, 189–194 (2015).
30. Negishi, J. *et al.* Porcine radial artery decellularization by high hydrostatic pressure. *J. Tissue Eng. Regen. Med.* **9**, E144–E151 (2015).
31. Chlupáć, J., Filová, E. & Bačáková, L. Blood vessel replacement: 50 years of development and tissue engineering paradigms in vascular surgery. *Physiol. Res.* **58**, 119–140 (2009).
32. Schoen, F. J. & Levy, R. J. Calcification of Tissue Heart Valve Substitutes: Progress Toward Understanding and Prevention. *Ann. Thorac. Surg.* **79**, 1072–1080 (2005).
33. Hendriks, M., Everaerts, F. & Verhoeven, M. Bioprostheses and its Alternative Fixation. *J. Long. Term. Eff. Med. Implants* **27**, 137–157 (2017).
34. Bussolati, G. *et al.* Acid-free glyoxal as a substitute of formalin for structural and molecular preservation in tissue samples. *PLoS One* **12**, e0182965 (2017).
35. Vito, R. P. The mechanical properties of soft tissues-I: A mechanical system for bi-axial testing. *J. Biomech.* **13**, 947–950 (1980).

36. Humphrey, J. D., Vawter, D. L. & Vito, R. P. Quantification of strains in biaxially tested soft tissues. *J. Biomech.* **20**, 59–65 (1987).
37. Billiar, K. L. & Sacks, M. S. Biaxial mechanical properties of the natural and glutaraldehyde treated aortic valve cusp - Part I: Experimental results. *J. Biomech. Eng.* **122**, 23–30 (2000).
38. Sacks, M. S. & Sun, W. Multiaxial Mechanical Behavior of Biological Materials. *Annu. Rev. Biomed. Eng.* **5**, 251–284 (2003).
39. Sun, W., Sacks, M. S., Sellaro, T. L., Slaughter, W. S. & Scott, M. J. Biaxial mechanical response of bioprosthetic heart valve biomaterials to high in-plane shear. *J. Biomech. Eng.* **125**, 372–380 (2003).
40. Stella, J. A. & Sacks, M. S. On the biaxial mechanical properties of the layers of the aortic valve leaflet. *J. Biomech. Eng.* **129**, 757–766 (2007).
41. Butler, D. L., Grood, E. S., Noyes, F. R., Zernicke, R. F. & Brackett, K. Effects of structure and strain measurement technique on the material properties of young human tendons and fascia. *J. Biomech.* **17**, 579–596 (1984).
42. Klinich, K. D. *et al.* Effect of frozen storage on dynamic tensile properties of human placenta. *J. Biomech. Eng.* **134**, (2012).
43. Todros, S., Pianigiani, S., de Cesare, N., Pavan, P. G. & Natali, A. N. Marker Tracking for Local Strain Measurement in Mechanical Testing of Biomedical Materials. *J. Med. Biol. Eng.* (2018). doi:10.1007/s40846-018-0457-z
44. Innocenti, B., Larrieu, J.-C., Lambert, P. & Pianigiani, S. Automatic characterization of soft tissues material properties during mechanical tests. *Muscles. Ligaments Tendons J.* **7**, 529–537 (2017).
45. Zwick/Roell. Zwick/Roell - Biaxial Test on Artificial Tissues. (2010). Available at: <https://www.zwickroell.com/en/medical/biomaterials-clinical-research/biaxial-triaxial-tests>.
46. Terzini, M. Exploring the mechanical properties of ex vivo human dermis in vitro and in silico. (2016).
47. Skulborstad, A. J., Swartz, S. M. & Goulbourne, N. C. Biaxial mechanical characterization of bat wing skin. *Bioinspiration and Biomimetics* **10**, 36004 (2015).
48. Johlitz, M. & Diebels, S. Characterisation of a polymer using biaxial tension tests. Part I: Hyperelasticity. *Arch. Appl. Mech.* **81**, 1333–1349 (2011).
49. Zemánek, M., Burša, J. & Děták, M. Biaxial Tension Tests with Soft Tissues of Arterial Wall. *Eng. Mech.* **16**, 3–11 (2009).
50. Sacks, M. S. A method for planar biaxial mechanical testing that includes in-plane shear. *J. Biomech. Eng.* **121**, 551–555 (1999).

51. Roland. ZSC-1 User's Manual.
52. ElectroForce. TestBench Series LM1 TestBench Test Instrument Reference Manual.
53. Black, M. M., Howard, I. C., Huang, X. & Patterson, E. A. A three-dimensional analysis of a bioprosthetic heart valve. *J. Biomech.* **24**, 793–801 (1991).
54. Krucinski, S., Vesely, I., Dokainish, M. A. & Campbell, G. Numerical simulation of leaflet flexure in bioprosthetic valves mounted on rigid and expansile stents. *J. Biomech.* **26**, 929–943 (1993).
55. Sung, H. W., Chang, Y., Chiu, C. T., Chen, C. N. & Liang, H. C. Crosslinking characteristics and mechanical properties of a bovine pericardium fixed with a naturally occurring crosslinking agent. *J. Biomed. Mater. Res.* **47**, 116–126 (1999).
56. Zeinali-Davarani, S., Chow, M. J., Turcotte, R. & Zhang, Y. Characterization of biaxial mechanical behavior of porcine aorta under gradual elastin degradation. *Ann. Biomed. Eng.* **41**, 1528–1538 (2013).
57. Rojo, F. J. *et al.* Optimal selection of biological tissue using the energy dissipated in the first loading cycle. *J. Biomed. Mater. Res. - Part B Appl. Biomater.* **95 B**, 414–420 (2010).